CHALMERS
UNIVERSITY OF TECHNOLOGY

3D scanning and printing of a triathlon bike for performance improvement.

A methodology and improvement proposal for a triathlon bike using reverse engineering and rapid prototyping

Master's thesis in product development

Akshay Mahadeva, Suraj Beejadi Satyanarayana

Department of Industrial and Material Science
CHALMERS UNIVERSITY OF TECHNOLOGY
Gothenburg, Sweden 2019

Master's thesis 2019

3D scanning and printing of a triathlon bike for performance improvement

A methodology and improvement proposal for a triathlon bike using reverse engineering and rapid prototyping

Akshay Mahadeva and Suraj Beejadi Satyanarayana

CHALMERS
UNIVERSITY OF TECHNOLOGY

Department of Industrial and Material Science
Chalmers University of Technology
Gothenburg, Sweden 2019

3D scanning and printing of a triathlon bike for performance improvement.
(A methodology and improvement proposal for a triathlon bike using reverse engineering and rapid prototyping)
Akshay Mahadeva, Suraj Beejadi Satyanarayana

Supervisor: Per Nyqvist, Research Engineer at the division of Production Systems.
Examiner: Björn Johansson, Professor at the division of Production Systems.

Department of Industrial and Material Science
Chalmers University of Technology
SE-412 96, Gothenburg
Telephone +46 31 772 1000

Cover: Illustration of different prototyping phases.

Typeset in LaTeX
Printed by Chalmers Reproservice
Gothenburg, Sweden 2019

Abstract

This thesis is conducted at Chalmers University of Technology, Gothenburg within department of Industrial and Materials science.

The project aims to develop a multi-purpose methodology for analysing and testing the developed prototype using a wind tunnel. Biking phase is considered in this thesis, since biking has the longest distance when compared to other phases. So, any small performance improvement in the biking phase will result in overall improvement. By performing an exploratory research and investigating the causes for performance improvement, methods such as rapid prototyping and reverse engineering are used.

The project resulted in analysing the impact of mounted accessories at two different positions. Results obtained from the testing phase are presented in terms of coefficient of drag and power required by the rider to overcome a certain range of velocity.

Preface

This report describes the process and results of the master thesis work which was performed until the period of Spring 2019. This master thesis is conducted by two students, aimed to create a suitable methodology for rapid prototyping and to disclose improvements that can be achieved from reverse engineering.

The thesis has been an interesting learning experience and we have met people with open helping hands along the way. A project that took longer than expected to deliver fruitful results, with continuous change in the path for problem solving. This gives us the opportunity to thank every one who shared their knowledge and assistance without which this thesis would not have been successful nor presented in this paper.

A special thanks to Hans Sjöberg (Research Engineer at the division of Production Systems) and Per Nyqvist (Research Engineer at the division of Production Systems) for continuously motivating and guiding us throughout the whole duration of the project and helping us in the most crucial stages of the project.

We would like to express our sincere gratitude to Jonatan Berglund (PhD student in the Department of Production Systems) for providing the necessary information regarding 3D scanning and helping to achieve the same.

We want to thank Isak Jonsson (Research engineer) for being our advisor and sharing his knowledge regarding fluid dynamics and wind tunnel testing.

We acknowledge our thanks to Björn Johansson (Professor at the division of Production Systems) for giving us the opportunity to conduct master thesis and providing feedback when necessary.

At last, we convey our heartfelt gratitude to all the people who have been continuous support for the project.

Akshay Mahadeva, Suraj Beejadi Satyanarayana. Gothenburg, September 2019.

Terminology

- ITU - International Triathlon Union
- CAD - Computer Aided Design
- CMM - Cordinate Measuring Machines
- DOF - Degrees of freedom
- CCD - Charged Coupled Device
- AM - Additive Manufacturing
- FDM - Fused Deposition Modelling
- SLA - Stereolithography
- SLS - Selective Laser Sintering
- STL - Standard Tessellation Language
- STEP - Standard for The Exchange of Product data
- PLA - Polylactic Acid
- ABS - Acrylonitrile Butadiene Styrene
- ASTM - American Society for Testing and Materials

Contents

List of figures

1
Introduction

This report represent the work and results that has been carried out, to find a solution for the improvement in the performance of a triathlon bike. The project is based on the wind tunnel testing of the chosen model. The chosen model is scaled down and 3D printed, to use as a test object in the wind tunnel.

1.1 Triathlon

Triathlon is a multi-sport athletic competition, where the athlete participates in different sport to complete the competition. It consists of three different sports conducted sequentially i.e. swimming, cycling and running. Time taken by the athlete to complete all three sport is considered as the total race time. Distance of each sport vary according to the race. Generally swimming has the shortest distance and cycling has the longest distance. In an ironman triathlon race the total distance to complete the race is 140.6miles, which is separated in to 2.4 miles(3.8 km) of swimming, 112 miles(180 km) of cycling and 26.2 miles(42.2 km) of running. Triathlon bikes are used in cycling event which are specially designed for this kind of race and are restricted to the international triathlon union (ITU). This bike has an additional handle known as aero handle. Since cycling has the longest distance to travel it is important to have a better performing bike to obtain better results.[1][2]

1.2 Project aim

The project aims to improve the performance of a triathlon bike by evaluating the mounted accessories on the triathlon bike.

1.3 Scope and deliverables

Lot of scientic research and time have been invested on aero-foil structure of triathlon bike since now athletes demand more efficient bikes to ride. Major of the triathlon bike manufacturers evaluate both user and the modified bike in the wind tunnel, but some manufacturers prefer a mannequin in the place of the user. Adjustable prototypes have been in use to instantly analyze the transition of flows. Till today importance is given to the bicycle frame and wheels for better performance, but not on the mounted accessories[3]. So, through this thesis importance will be given to the mounted accessories.

Thesis should conclude in terms of:

1. A scaled physical prototype

2. Digital models obtained from scanning
3. Results and analysis on performance of the triathlon bike with different configurations.

1.4 Constraints

The chosen solution should meet the standard requirements, which might hinder the possibility to assign major changes to the bike. Considered constraints are mentioned below,

- Specific model of a triathlon bike will be considered for testing.
- The bicycle frame and wheels are considered to be constant.
- The overall dimensions and design of the bike should be according to competitive rules by International triathlon union(ITU).

The developed solution should be considered as a research suggestion and guideline for carrying out the reverse engineering and wind tunnel testing of the developed prototype.

2
Background Information

This chapter contains all the literature research and additional information that serves as a base to understand and interpret the results throughout the project duration.

Theoretical background

2.1 Reverse Engineering

Engineering is process of designing, developing and maintaining the product. This is known as conventional or forward engineering. Reverse engineering is a process of extracting the knowledge of the existing product. Reverse engineering serves as a great tool, when there is no information available other than the physical product. If a product needs to be duplicated or to be developed further but the data or drawing is missing, in such cases reverse engineering helps to extract the details of the product. In reverse engineering the details are obtained as 3D points of the product by scanning using a 3D scanner. Obtained 3D points are then converted into solid or surface model using CAD software. The obtained solid or surface model is used to develop the product further.[4]

2.2 3D Scanning Data and meta data collection

There are several methods available for scanning a 3D object, which in turn can be stored as data to be used in different applications including rapid prototyping and 3D reconstruction. In this project data refers to the information obtained from the scans performed using a scanner and meta-data refers to number of cloud points and their coordinates w.r.t global coordinate system.[5] [6]

2.3 Methods of 3D data acquisition

There are several methods available for scanning a 3D object or a geometric item, some of the methods are presented below. Further, scanning can be broadly classified into contact technique and non contact technique.

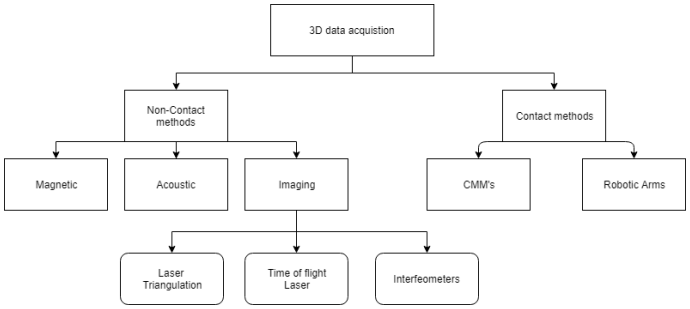

Figure 2.1: Classification of 3D scanning methods [5]

2.3.1 3D scanners and point clouds

- **3D scanners**

  All the devices that are capable of obtaining the 3D coordinates of a geometric item and storing it in a structured feasible manner are considered as a 3D scanning device. A 3D scanner can be defined as "any device that collects three dimensional coordinates of a of a given region of an object, in a systematic pattern at a high rate achieving the results in real time". 3D scanners involve various techniques that needs to be employed depending on the size, shape and the surface area that needs to be scanned. Even the distance at which the scans has to be done should be predetermined. 3D scanners are used in various fields and have different technical purpose. Most common of them are used in quality control of production lines, reverse engineering, airborne topological scans and rapid prototyping.[7]

- **Point clouds**

  Point cloud is the result of probing a three dimensional object, typically they are cluster of data points present in the space w.r.t the 3D coordinate systems. Point cloud are mainly used for 3D reconstruction using CAD. Some of the other applications include visualization and quality inspection.[8]

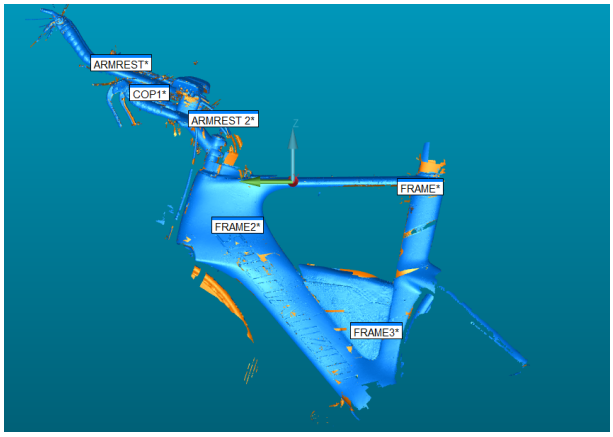

Figure 2.2: Point cloud obtained from scanning

2.3.2 Tactile contact method

In this method, the scanner is in direct contact with the 3D object. The scanner contains an arm which can be controlled either manually or automatically. The object to be scanned is placed on a secured firm platform and a mechanical arm is fitted with a probe at the free end. The arm needs to be calibrated for every new 3D object placed on the platform. When the probe is in contact with the 3D object obtained data is stored as points and geometric features, which in turn can be converted into 3D mesh. One of the best example of tactile contact measuring device is coordinate measuring machines (CMM's), CMM's are frequently used in manufacturing industry to measure the error in the different batches produced. This method is not used most commonly due to the fact it has slow scan rates and it might tend to move the object fixed on the platform which might hinder the result obtained. Since the scans are obtained in the form of X,Y,Z coordinates of the object any disturbance or minute movement will result in irregular surfaces. Main industrial applications includes dimensional measurement and digitizing the physical object.[6] [9]

2.3.3 Non contact method

3D scanners of this type does not make any kind of physical contact with the object. This method relies on moving the scanner around the 3d object in all the possible directions to get a digitized model or point clouds. This method is dependent on either non contact active technique or non contact passive technique to scan a 3D object. The object to be scanned is placed on firmly on a fixed platform. Whereas, the scanner can be moved around freely in six dof's. Point clouds obtained from scanning is used in various applications such as reverse engineering, engineering analysis and rapid prototyping for testing applications. Two techniques involved in scanning is briefly explained below.[7]

2.3.4 Non contact active method

Non contact active method scanners use light or some sort of radiation to probe an object and an active sensors to detect reflection. Types of commonly used radiations for non contact active probing include light, ultrasound, and x-ray. Non contact active scanners that use radiations are grouped into three major categories namely time of flight, phase shift and laser triangulation. In most cases scanning techniques are used individually for scanning but is some cases more than one technique is used in conjunction with the other.[7]

- **Time of flight scanners**

  This technique is based on the time consumed for transmitting and reflecting the signal from the object. Working principle of this technique relies on sending back and forth a certain type of radiation(for example laser pulse) between a transmitter and reflecting surface, then the total time taken for the signal transmission and reception is calculated. Scanners of this type are capable of scanning points that are present in its field of view one at a time so the scanner can have the whole field of its view by manipulating receptors field of view. Time of flight scanners are capable of scanning approximately 10,000 to 100,000 points per second. Since the operating distance between the object and scanner is short, accuracy during the whole scan

duration remains the same. Low resolutions scans are easily achievable with less time whereas high resolution scans take more time because of increase in number of sample points.[7] [9]

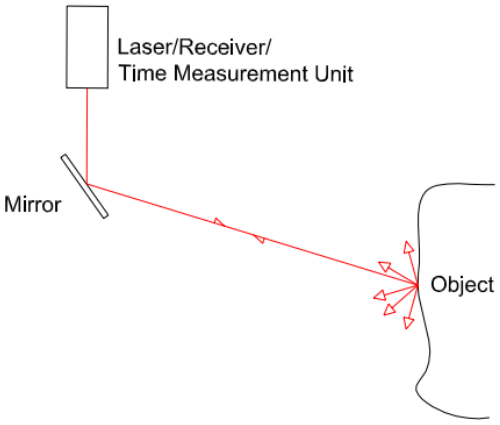

Figure 2.3: Illustration of triangulation scanning method [9]

- **Phase shift scanners**

  Phase shift scanners uses laser pulse as a source to detect the distance travelled between object surface and the scanner. In this technique a laser pulse is emitted from the transmitter of the scanner to the object surface, the signal returning from the surface is then stored and analyzed with the emitted signal to calculate the shift in phase between the emitted and received signal. Precision of the results depends on the frequency of the laser pulse i.e. precision increases with higher frequency and shorter distance. Since it involves complex signal analysis, obtained cloud points or more accurate. Also, this type of scanner has reduced range due to the fact an accurate returning signal is needed to compute the difference. Phase shift scanners are more faster compared to time of flight scanners so it might produce more unnecessary points in the object space if the range of the scanner is increased.[7] [9]

- **Triangulation scanners**

  This method uses laser light to probe the surface of the object to be scanned. In this technique the laser light, charged coupled device camera(CCD) and laser emitter will form a triangle while scanning, hence the technique is named as triangulation. A CCD camera is a device that is able to convert light signal in to digital data using the lens. As shown in figure 2.4 the distance between the laser emitter and camera are known including the distance between emitter and the object. The unknown distance between the CCD camera and object surface is later calculated depending on the angle of contact of the laser beam. The light reflected back from the object surface is then collected through the field of view of the lens as a light signal which is later converted into 3D digital data. This type of scanner requires both the object and scanner base to be fixed on sturdy platform to avoid any types of disruptions and noises caused during the scanning process.[7] [9]

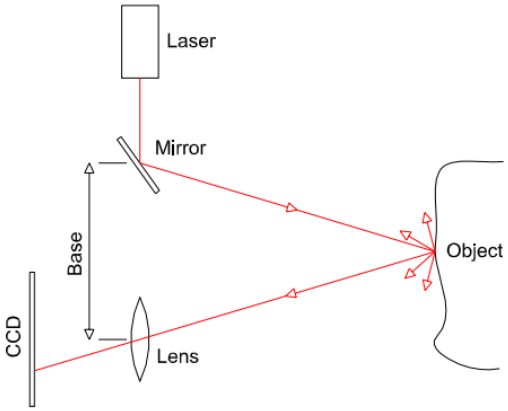

Figure 2.4: Illustration of triangulation scanning method [9]

2.3.5 Non contact passive method

Scanners of this type does not use any kind of light pulse for probing the object surface, they rely on natural light surrounding the object. Techniques involved in this method are simple when compared to active scanners because they capture the object in digital format in presence on natural light. Most used non contact passive scanners are video cameras and digital cameras.[7]

2.4 Model Reconstruction

Obtained point clouds from the scanners can be used to generate either a mesh model or a CAD model depending on the application. The whole process of developing the point clouds into a structured feasible model is called model reconstruction. The point clouds cannot be used directly for reverse engineering or rapid prototyping so point clouds are generally converted to different modelling formats.[10]
The 3 most feasible models for creating prototypes are presented below:

- **Polygon mesh models**

  Polygon mesh models consists of vertices, edges and faces as an integral part of the produced 3D shape. The number of vertices and triangles that are present in the model depends on size and shape of the scanning object. Generated mesh model of this type are usually large due the fact they contain large number of data sets representing them. Conversion from point cloud to mesh model is done by joining adjacent point in the point cloud which in turn creates a continuous surface. Joining of the adjacent point is done by algorithms in the software applications(e.g. MeshLab, Cloudcompare).[11] [12]

- **Surface models**

  Models of this type consists of NURBS, T splines or wire frames having other forms curved topology. All the curve topologies are dependent on mathematical expressions to form a surface model collectively. Obtained point clouds can be converted into surface models with the aid of software applications which can create curves

between the points and then create an external surface based on the curves. In most cases the resulted surface from the application software are not smooth and they may require some patching operations to even out the surfaces. A Majority of the software application offer both manual and automated patching for the created surfaces. Compared to polygon mesh models, surface models are lighter because of the wire frame structure.[10]

- **Solid models**

  Solid models represents the data in the form of edges, faces and details regarding the structure of the object on the exterior surface of the model. In addition to this solid models consists of wire frame as an integral part. Point clouds can be either converted directly in to a solid model or can be converted to a surface model after the patching operation. Most industrial application requires a solid model in the form of CAD geometry since it represents the geometric features of the object being scanned. This model offers the flexibility to perform boolean operations and parametrization on the built CAD geometry. Complex shapes are achieved in solid modelling by combining primitive shapes. Most of the CAD based applications are able to process the solid models because they are robust and made up of primitive shapes.[13]

- **Primitive shapes**

  Primitive shapes are fundamental solid objects that posses mathematical boundary representations.

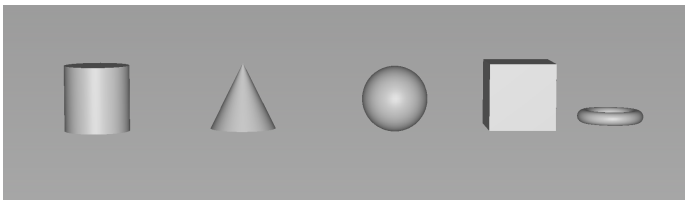

Figure 2.5: Examples of primitive shapes obtained form Alias AutoStudio

2.5 3D printing

3D printing also known as Additive manufacturing, is a rapid prototyping process where the materials are added layer by layer to build the model. The name additive manufacturing is used since, the parts are printed by adding one layer upon the other layer. Complex designs are built easily because it offers a high degree of freedom for prototyping. Due to ease of complex design printing, 3D printing avoids the assembling of the part, the tool and the cost associated to assembly compared to other manufacturing process. There are different technologies used for 3D printing which are stated below.

1. **Fused Deposition Modelling**

   Fused Deposition Modelling(FDM) is the most common type of 3D printing technology used. The process of printing the model is by heating the material and

extruding the material through a nozzle to print it on the print bed. This technology is generally used for prototyping purpose. Figure 2.6 shows the technology of the fused deposition modelling.

2. **Stereolithography**

   Stereolithography(SLA) is another 3D printing technology which uses light source as laser and vat resin to build the model. The process of printing the model is by initiating the laser beam on to the surface of the vat resin to start the polymer chain. This chain reaction helps to have strong bond and form the solid model. Figure 2.7 shows the technology of the stereolithography.

3. **Selective Laser Sintering**

   Selective Laser Sintering(SLS) is another 3D printing technology which uses laser and powder to build the model. The process of printing the model is by initiating the laser beam on to the powder bed of the material. It sinters the powder particle to each other to form the solid model. Figure 2.8 shows the technology of selective laser sintering.[14]

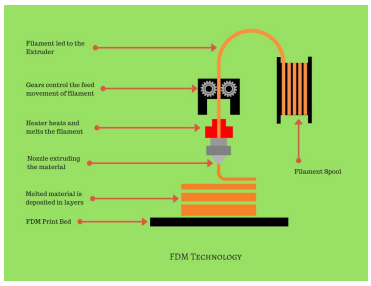

Figure 2.6: FDM[15]

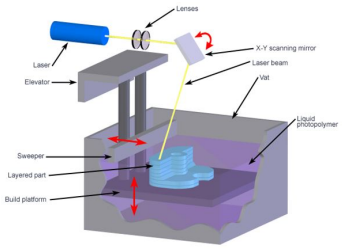

Figure 2.7: SLA[16]

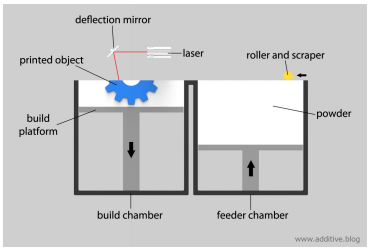

Figure 2.8: SLS[17]

2.6 Fluids and flow types

2.6.1 Types of fluids

For easier analysis over different varieties of fluids, fluids are divided into 5 major classes[18]

1. Ideal fluid
Fluids of this type are incompressible and have zero viscosity. Ideal fluids does not exist in nature

2. Real fluid
Any fluids having viscosity greater than zero are called real fluids. All the fluids available in nature are real fluids.

$$\mu > 0 \tag{2.1}$$

3. Newtonian fluid

These are real fluids in which shear stress is directly proportional to the rate of shear strain (Velocity gradient).

$$\tau = \mu(\frac{du}{dy}) \tag{2.2}$$

where,
τ = Shear stress
μ = Viscosity if the fluid
$(\frac{du}{dy})$ = Coefficient of viscosity

4. Non-newtonian fluid

Non Newtonian fluid posses viscosity greater than zero, in this type of fluids shear stress is not directly proportional to the rate of shear strain.

5. Ideal plastic fluid

This type of fluid shear stress is greater than the yield value and shear stress is proportional to the rate of shear strain.

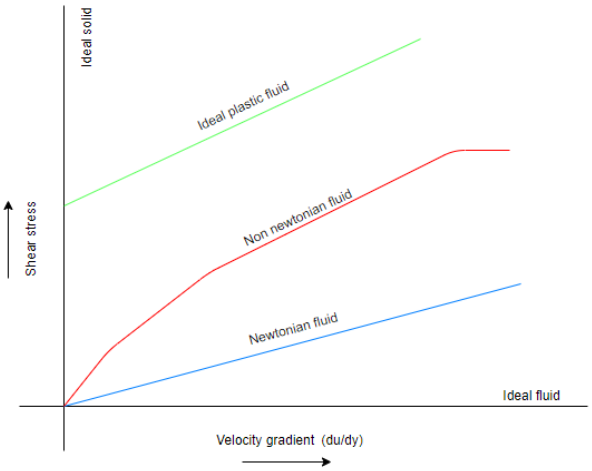

Figure 2.9: Types of fluid w.r.t to shear stress and velocity gradient [18]

2.7 Kinematics of flow

2.7.1 Types of flow

In fluid dynamics, fluids are segregated into six major categories namely:[18]

1. **Steady and Unsteady Flows**

   In steady flow, the governing characteristics of the fluid like velocity , pressure(p) or density(ρ) does not change with respect to time. It can be represented as follows

$$(\frac{\delta v}{\delta t})_{x_0,y_0,z_0} = 0, (\frac{\delta p}{\delta t})_{x_0,y_0,z_0} = 0, (\frac{\delta \rho}{\delta t})_{x_0,y_0,z_0} = 0 \tag{2.3}$$

In unsteady flow the velocity, pressure or density at any point at a given instant changes continuously with respect to time.

$$(\frac{\delta v}{\delta t})_{x_0,y_0,z_0} \neq 0, (\frac{\delta p}{\delta t})_{x_0,y_0,z_0} \neq 0, (\frac{\delta \rho}{\delta t})_{x_0,y_0,z_0} \neq 0 \tag{2.4}$$

Where,
(x_0, y_0, z_0) is a fixed point in the fluid stream.

2. **Uniform and Non-uniform Flows**

In uniform flow the velocity of the flow does not change with respect to the distance travelled by the fluid in a given direction.

$$(\frac{\delta v}{\delta s})_{t=constant} = 0 \tag{2.5}$$

If the velocity of the flow keeps on changing with distance traveled by the fluid in any given direction, then these type of fluid are non-uniform in nature.

$$(\frac{\delta v}{\delta s})_{t=constant} \neq 0 \tag{2.6}$$

Where,
δv = Change in velocity
δs = Distance travelled by fluid in given direction.

3. **Laminar and Turbulent Flows**

In laminar flow, fluid particles travel along a straight line and will remain parallel for the whole duration of the flow. Laminar flow is caused due to the fluid particles traversing smoothly in horizontal direction.

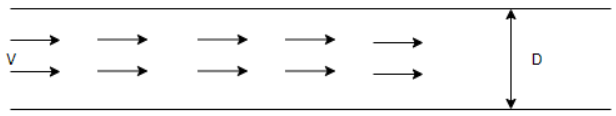

Figure 2.10: Illustration of laminar flow

Turbulent flow consists of disoriented and unorganized fluid particles, which tend to follow random path during the whole duration of the flow. The energy losses are high in this type of flow, because of the resistance between adjacent layers.

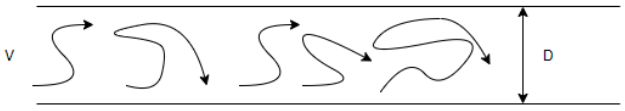

Figure 2.11: Illustration of turbulent flow

Type of flow of a fluid can be determined by dimensionless number called Reynolds number,

$$Re = \frac{vD}{\nu} \tag{2.7}$$

Where,
D = Diameter of the flow space.
v = Velocity of the fluid in the space
ν = Kinematic viscosity of fluid.
Depending on the range of the Reynolds number, the flows can be either identified as laminar or turbulent. For laminar flow Reynolds number(Re) should be less than 2300 and for turbulent flows it should be more than 2900. If the value lies in between 2300 to 2900 then flow may be either laminar or turbulent.

$$Re < 2300\ (Laminar flow) \tag{2.8}$$

$$Re > 2900\ (Turbulent flow) \tag{2.9}$$

4. **Compressible and In-compressible Flows**

If the density(ρ) of a fluid keeps on changing constantly at any given point in the flow then it is called compressible flow.

$$\rho \neq Constant \tag{2.10}$$

In in-compressible flow, the density of the fluid remains constant throughout the duration of the flow.

$$\rho = Constant \tag{2.11}$$

5. **Rotational and Irrotational Flows**

In rotational flow, fluid particles following a certain direction tend to rotate about their own axis. Similarly, if the fluid particles flowing in a certain direction does not tend to rotate on their own axis then that flow is irrotational flow.

6. **One, Two and Three Dimensional Flows**

In one-dimensional flow, there exist a single parameter which has a function in one space coordinate. When considering a steady one-dimensional flow, velocity of the fluid is dependent on function along the x-coordinate. So one-dimensional flow can be expressed as velocity "u" as the function of "x" coordinate. Variation in velocity in two other directions are neglected since they are mutually perpendicular.

$$u = f(x), \nu = 0\ and\ w = 0 \tag{2.12}$$

Where u, ν and w are velocity components in x,y and z directions respectively.

In two-dimensional flow, flow is dependent on function along two coordinates in

the fluid space. Variation of velocity in "z" direction is considered to be negligible. So, flow can be expressed as velocities "u" and "v" as function of "x" and "y" coordinates respectively.

$$u = f_1(x, y), \nu = f_2(x, y) \; and \; w = 0 \tag{2.13}$$

In three-dimensional flow, the velocity is completely dependent on three axes which are mutually perpendicular to each other. So, steady three-dimensional flow can be expressed as velocities "u", "v" and "w" as function of three coordinates "x", "y" and "z" respectively.[18]

$$u = f_1(x, y, z), \nu = f_2(x, y, z) \; and \; w = f_3(x, y, z) \tag{2.14}$$

2.8 Bluff bodies

Bluff bodies are three-dimensional design structures (or objects), when immersed in a flow stream has substantially separated flow over its frontal area which in turn causes non-uniformity in the direction of the downstream flow. Bluff bodies can be easily distinguished in any flow due to the fact they have lower aerodynamic loads when compared to other bodies and that are capable of creating disruption in the flow. Three-dimensional bluff bodies have lower aerodynamics load because there might be a chance of flow in the other direction which tends to modify the flow structures due to vortex and wake formation behind the bluff bodies.

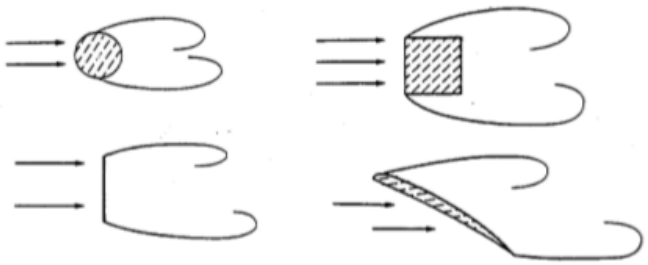

Figure 2.12: Example of bluff bodies [19]

Nowadays, most of the objects or shapes that are being tested in the wind tunnel are bluff bodies. Bluff bodies always give rise to different types of flow configurations and higher number of variables affecting the flow. This makes it difficult to analyze from the data that is already available as research. So, it is always inevitable to rely on the experimental data rather than theoretical data in the case of bluff bodies.[19]

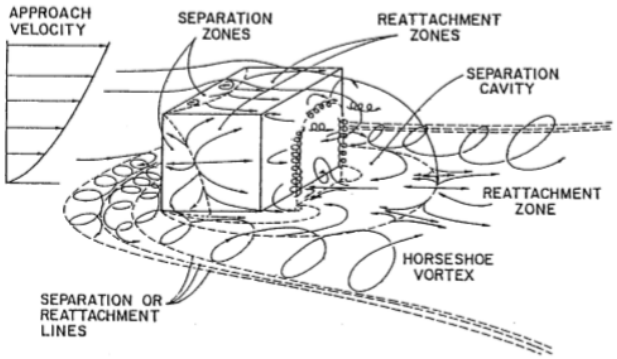

Figure 2.13: Illustration of flow around 3-dimensional bluff body[19]

2.8.1 Bluff body aerodynamics

When considering a bluff body immersed in a flow stream the boundary layers tends to isolate from outer edges. Most commonly boundary layer separation takes place at the surfaces with maximum area. Boundary layer separation takes place due to less reduction of body width towards downstream flow. This causes huge pressure difference behind the body, which leads to the creation of wake vortexes.

Figure 2.14: Illustration of vortex formation behind a bluff body[19]

In most cases, when a body is submerged in fluid with a flow velocity(U) the body will experience both tangential and normal stresses over the exposed surfaces. Resultant of this stresses can be expressed by means of force and moment coefficients.[19]

$$C_{F_i} = \frac{F_i}{\frac{1}{2}\rho u^2 S}; \qquad C_{M_i} = \frac{M_i}{\frac{1}{2}\rho u^2 S l} \tag{2.15}$$

Where,
C_{F_i} and C_{M_i} are dimensionless quantities namely force coefficient and moment coefficient.
F_i and M_i are the components of the resultant force and moment along the given direction
$\rho \Rightarrow$ density of the given fluid.
$u \Rightarrow$ flow velocity of the fluid.
$S \Rightarrow$ reference surface.
$l \Rightarrow$ reference length.

2.9 Wind tunnels

Wind tunnels play an important role generating experimental data for analyzing the influence of the wind on any scaled object. In this project, experiment is conducted at

low speed and is not completely dependent on complex fluid parameters. Wind tunnels are most widely used to analyze the performance of the scaled models. Low-speed wind tunnel can provide valid data that can be used as basis for improvement in design phase. Performance of the scaled object can be determined by generated aerodynamic data which helps to make critical decisions for initiating design change. [20]

2.9.1 Types of wind tunnels

- **Open circuit wind tunnel**
  In open circuit tunnels the wind generally flows in a straight path. It consists of contracted inlet from where the air flow begins, a diffuser, a fan section and an outlet for the generated wind. More often this type of tunnels either consist of a concealed space (Closed jet) for testing the object or without a specific boundary (Open jet). For open circuit closed wind tunnel refer figure 2.15.[20]

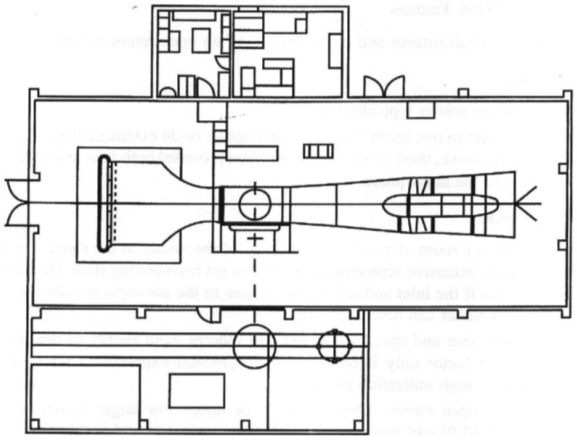

Figure 2.15: Plan view of an open circuit wind tunnel (Diamler-Benz Aerospace Airbus, Bremen, Germany).

- **Closed circuit wind tunnel**

  Closed circuit wind tunnels (figure 2.16) works on the principle of loop, where air generated does not leave the tunnel. The air inside keeps on recirculating for the whole duration of testing with minimal exchange of air with surroundings. The flow parameters can be regulated easily due to the presence of vanes and screens for redirecting the flow. Efficiency of the closed circuit wind tunnels is higher when compared to open circuit tunnel because of the minimal or zero interaction with the atmospheric air.[20]

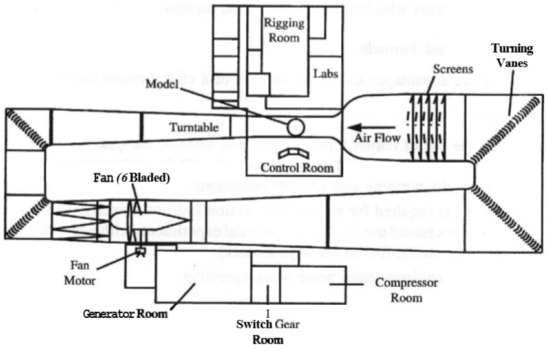

Figure 2.16: A closed circuit wind tunnel, Defense Establishment Research Agency (DERA), 13 X 9-ft tunnel in Bedford, England.

The wind tunnel used for testing the developed prototype is located at Chalmers, which is a semi-closed wind tunnel. This wind tunnel is powered by a 180 kw motor, which generates the wind at atmospheric pressure. Several shapes and sizes of geometries can be easily tested because of the mounting and traversing systems present in the wind tunnel.

2.9.2 Force and moment measurement

Fundamental aspect of a wind tunnel testing is to measure and estimate the amount of steady and unsteady forces acting on a body placed in the flow. To determine the amount of steady forces acting on a body strain gauge balances are commonly used. Similarly, piezo sensors are used for unsteady measurement of forces. Due to high rigid property of piezo materials they induce or have zero interference with independent force components. Materials with high rigidity have high natural frequencies, which eliminates the interference caused due to unsteady flows in aerodynamics. The major measurement device in any wind tunnel is a multi component force and moment measuring system, which consist of transducers, strain gauges and piezo electric sensors. Usually strain sensor in strain gauges with resistance foil and piezo balances consists of semiconductor gauges.[21]

2.9.2.1 Balance types

Balance types can be broadly classified into two major categories, depending on the position balances are placed. If the balance is placed internally in the model during testing then it is referred to as internal balance (figure 2.17), where as if the balance is located outside the model they are called external balances (figure 2.18). Both specified types of balances are able to measure multiple force and moments concurrently.[21]

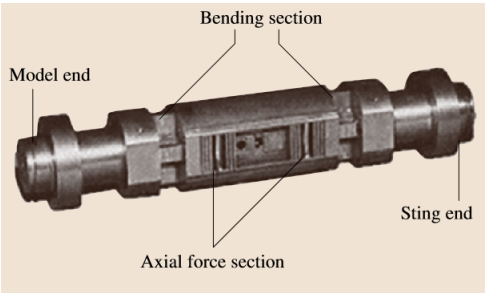

Figure 2.17: Typical internal balance [21]

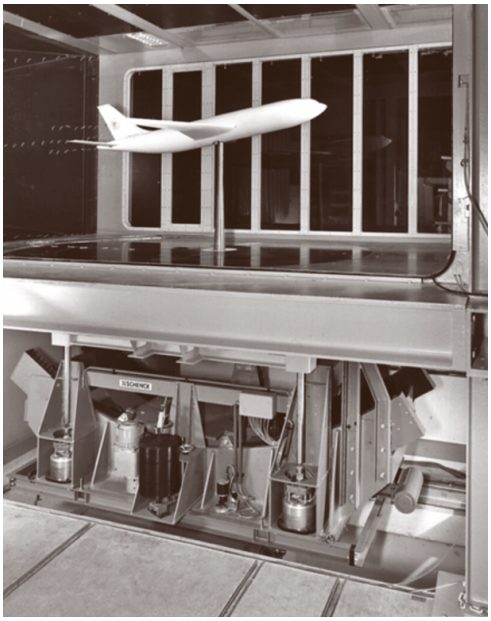

Figure 2.18: External balance and support [21]

3
Methodology

For analyzing the chosen triathlon bike and its performance there is a need for both a 3d printed prototype and a solid cad model for 3d printing. The model serves as a basis for testing in the wind tunnel. Instead of a real user and bike a prototype of the original bike and the user is used. So to obtain the prototype 3D scanning is used to create the digital replica of the bike and the user. The other way to create a prototype is to manually create a CAD model using the scanned data as a reference in the CATIA V5.

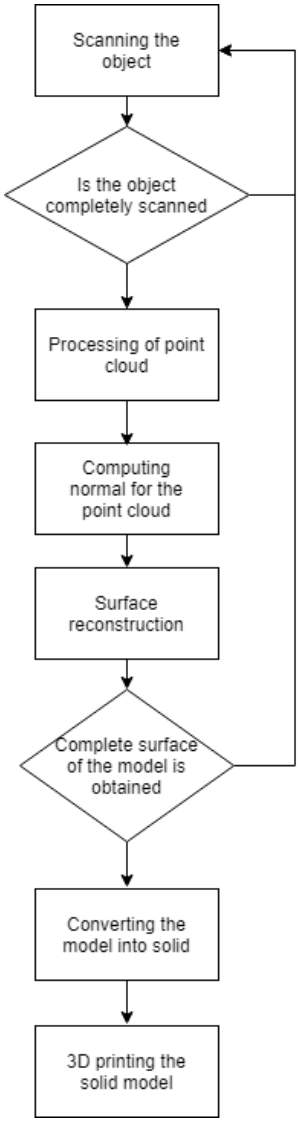

Figure 3.1: Methodology used for reverse engineering

3.1 Scanning the object

3.1.1 Laser scanning

To obtain the point clouds one of the method employed is 3D Laser scanning, by using a laser probe. Measurement software used is PC-DMIS, developed by Hexagon manufacturing intelligence. The romer arm has six degrees of freedom, the frontal part of the arm accommodates for various tools that can be used for measuring coordinates and scans. For the purpose of 3D scanning a laser probe is used, which contains a laser emitter, camera and led lamp. Depending on the surface color of the object being scanned, intensity of the laser needs to be changed accordingly. For example if the object has darker surface intensity of laser probe needs to be higher, where as for the lighter surface intensity should be lowered significantly.

(a) Image of laser probe [22]

(b) Image of romer arm with six DOF [22]

The bike was placed in such way that it is accessible in all the ways for scanning using romer arm. The bike is mounted on two supporting structures one in the front and one at rear wheel. For the whole process of the scanning the bike remained stationary since any small movement would affect the scanning in terms of cloud point accuracy. Also, any change in position of the scanning object will result in inappropriate surfaces. If the scan has multiple different individual point clouds they can be combined by copying the text files from one file to another.

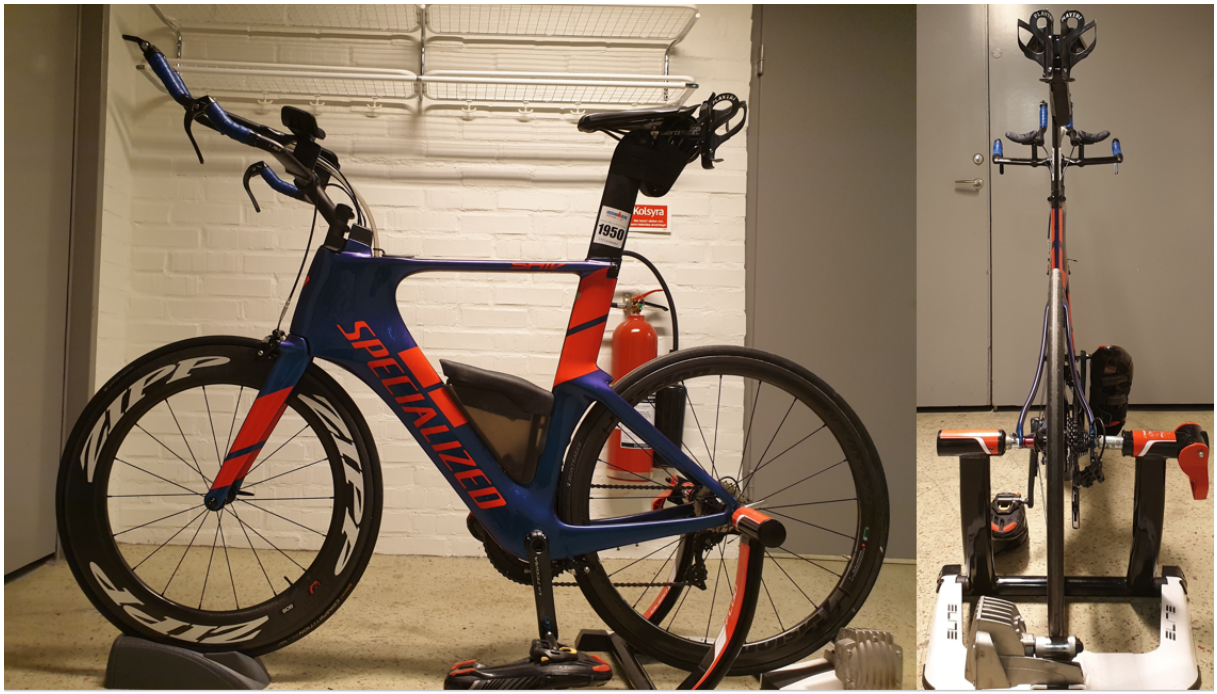

Figure 3.2: Triathlon bike mounted on supports during scanning

3.1.2 Hand-held scanning

In addition to laser scanning, a hand held scanning session was conducted to support the prototyping process. This method involves keeping the subject/object stationary in the centre and revolving around the object with the hand held scanner for the whole duration of scan. Depending on the structural complexity of the object and environment lighting condition scanner should be adjusted accordingly. Common practice is to do multiple scans around the object to obtain most accurate results. Obtained point cloud points from scanning was filtered and converted into water tight mesh model for importing and carrying out operation in CATIA V5.

(a) Point cloud of the scanned object

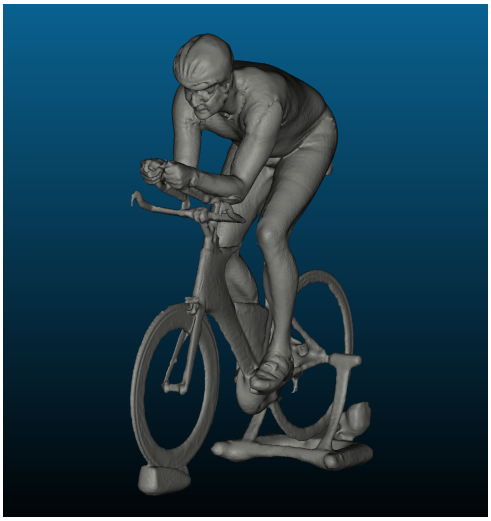

(b) Water tight mesh model of the obtained point clouds

3.2 Processing of point cloud

Once scanning has been done, obtained point clouds needs to processed for model construction and surface Reconstruction. There are several pre-processing software available in the market but software programs used in this project are MeshLab and cloud compare. For surface reconstruction the software programs used are Catia V5 and Autodesk Meshmixer.

3.2.1 Filtering and operations

The scanned results are obtained in the form of point cloud, point cloud can be either edited as surface models or as text files which represent the x-y-z coordinates. Filtering is the process of removing unwanted data from the obtained data for performing further experimental analysis. In this case the data obtained is in the form of point clouds which contains a scanned 3D cluster of points which represent the scanned object.

3.2.2 Cloud compare

Cloud compare is a 3D point cloud processing software which is capable of handling triangular meshes and performing Boolean logic operations on the given point clouds. There are several methods to combine the obtained clouds one of the major used method is to combine point clouds based on alignment from one cloud to the other. Here, Cloud compare is mainly used to filter the unwanted point from the cloud and generate mesh for post processing. The obtained point cloud is opened with suitable file format in cloud compare to perform operations. The first step is to remove the points which have been generated outside the object space. So as to remove irregularities while meshing. This can be done using the operation present in cloud compare.

3.2.2.1 Boolean logic operations

In cloud compare the obtained point clouds, were loaded in the form of *.txt* file format. After loading the points, the points were tab delimited and was converted to ASCII file format. Once ASCII file format is obtained simplification operations such as sub-sampling of the point clouds is performed. Sub-sampling helps to reduce the number of points present at a surface through computing normals, which in turn decreases the amount of points that are unnecessary at clusters if there have been multiple scans of the same surface. Reduced point clouds are lighter and simplification operations can be performed at greater speed.
If an object is scanned in two sets and point clouds of both sets needs to combined, the reduced point clouds can be combined with other point clouds to obtain a complete point cloud set. Given the condition object has remained stationary and stable throughout the performed scanning sets.

3.3 Computing the point cloud

As the point clouds are filtered and cleaned, these point clouds needs to be meshed in order to reconstruct the model. To mesh the point clouds, the file is imported to a meshing software called MeshLab. MeshLab is an open source software system used for processing

and editing of the 3D meshes. In MeshLab, the point clouds file is imported as PLY format. PLY format is known as the polygon file format which stores the three-dimensional data obtained by the 3D scanner. As the file is imported, the point cloud need to be computed for surface normal. Surface normal is a vector which is perpendicular to a series of point within the point cloud. In this, set of neighbouring points are used to estimate the normal. It is possible to set the number of neighbouring points required to compute the normal. Figure 3.3 shows compute of the normal using the neighbouring sum of 10.[23] [24]

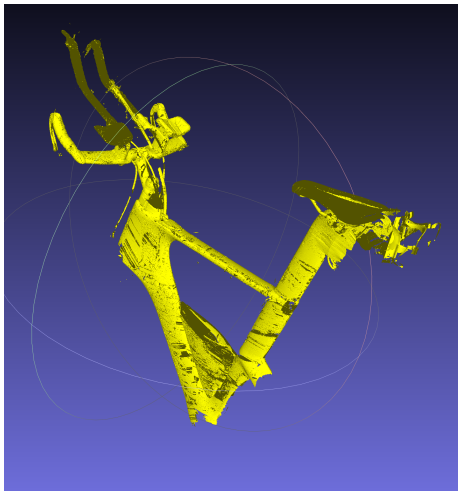

Figure 3.3: Computing normal to the point cloud

3.4 Surface reconstruction

After computing, the normals are used for surface reconstruction. Surface reconstruction is carried out by Poisson surface reconstruction. Poisson surface reconstruction is an approach used to generate the surfaces from the points and the normals generated. Generated surfaces are in the form of high-density triangulated mesh. The density of the mesh or the surface reconstruction can be controlled by reconstruction depth. Reconstruction depth is used to extract the final surface, higher the value of reconstruction depth high resolution surface is obtained. During the surface reconstruction unwanted meshes are generated, which needs to be deleted for further processing. Figure 3.4 shows the mesh using Poisson surface reconstruction having a reconstruction depth of 10 and the unwanted meshes generated are deleted.[24]

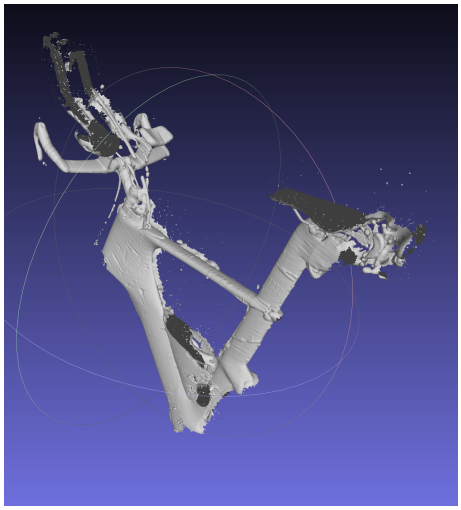

Figure 3.4: Surface reconstruction from normal and points

3.5 Converting the model into soild

The mesh file obtained is exported to Meshmixer in STL file format. Meshmixer is an open source software system used for editing the model. The mesh file is imported into meshmixer where the model is converted into a solid. Figure 3.5 shows the solid model of the bike that is converted from the mesh imported. This solid model is exported for 3D printing in STL format.[25]

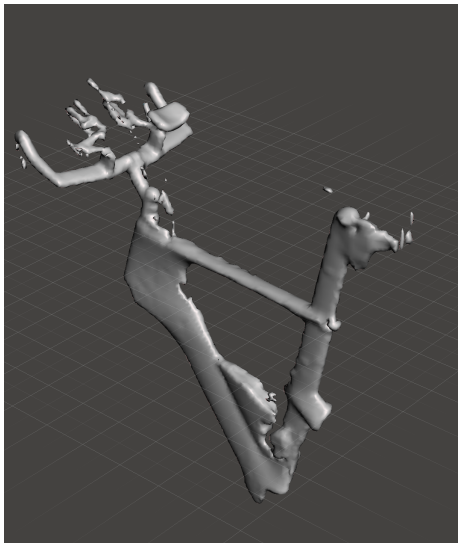

Figure 3.5: Solid model converted from the mesh

3.6 Challenges in surface reconstruction

The method approached for converting the model from point clouds to solid 3D model was successful. Still, the model could not be printed as it had many gaps in the model which could not be solved in the MeshLab or Meshmixer. From the figure 3.5 it can be seen

that there are many parts that are not completely converted into a solid. In this model the aero handle, seat are missing and there are few gaps found in the frame structure. The reason for the gaps obtained in the model is due to the inappropriate 3D scanning of the bike. As the bike was at stationary, it was difficult for the arm to scan it thoroughly. This lack of complete scanning of the bike caused the gaps in the model which was not suited for 3D printing. To continue with the project a similar bike CAD model is taken from the GrabCAD and used for prototype purpose.

4

Engineering Design and Prototyping

The model for 3d printing is obtained from GrabCAD and changes on the model is made depending on the requirements generated. Most of the geometrical features and surfaces are added through the iterative process in CATIA. The full scale of the model is difficult to 3D print and test in the wind tunnel due to which model is reduced to 60% i.e. the model that is printed and tested is 40% of the original model. Since the build volume of the printer is limited, the total size of the reduced model exceeds the printer dimensions. So, the model is divided into several smaller parts by splitting so that the parts can be printed without exceeding the printer dimensions. While dividing the model, critical joints are considered in order to obtain a strong bond between the parts. Figure 4.1 show the different views of the complete model.

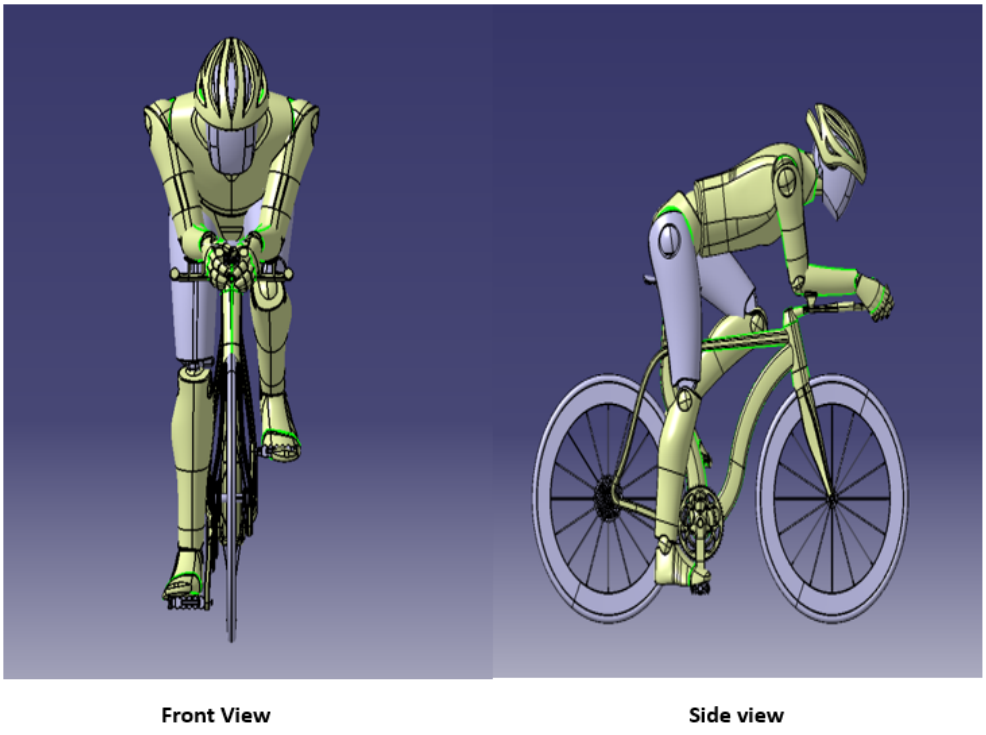

Figure 4.1: Different views of the complete model

4.1 Development of Prototype

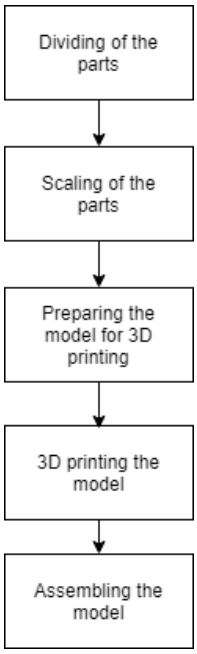

Figure 4.2: Development process of the prototype

4.1.1 Dividing

The model is divided into several smaller parts by splitting and trimming of the reduced model. While dividing the model, supports structure obtained to build the parts are taken into consideration. The frame is the biggest part which must be divided into smaller once. Initially, a rectangle of the suitable dimension for printing is drawn and used to pocket the remaining parts such that only the required smaller part is remained. These smaller parts are then divided in two half using split operation as it would be useful to print the parts. After splitting, the parts are trimmed in order to eliminate the unwanted surface obtained during splitting. Extra detailing as holes is drilled in the model to hold the spilt part and be in line. All the operations of splitting and trimming are done in generative shape design workbench. The part in the figure 4.3 shows the process of splitting where the part is split into two parts. The complete centre part of the frame is shown in (a), a line is drawn and extruded it to the complete part shown in (b). Using split option the complete part is split into two parts with respect to the extruded line. Unwanted surface are removed by trim and holes are drilled to hold the model each other inline as shown in (c). In similar way different parts are divided and made into smaller parts. Another difficult part to print is the user where a mannequin is used. The mannequin is divided into smaller part by splitting at different joints. The upper body is split into two halves. The hands are divided at the shoulder joint, elbow joint and wrist joint. The legs are divided into knee joint and ankle joint.

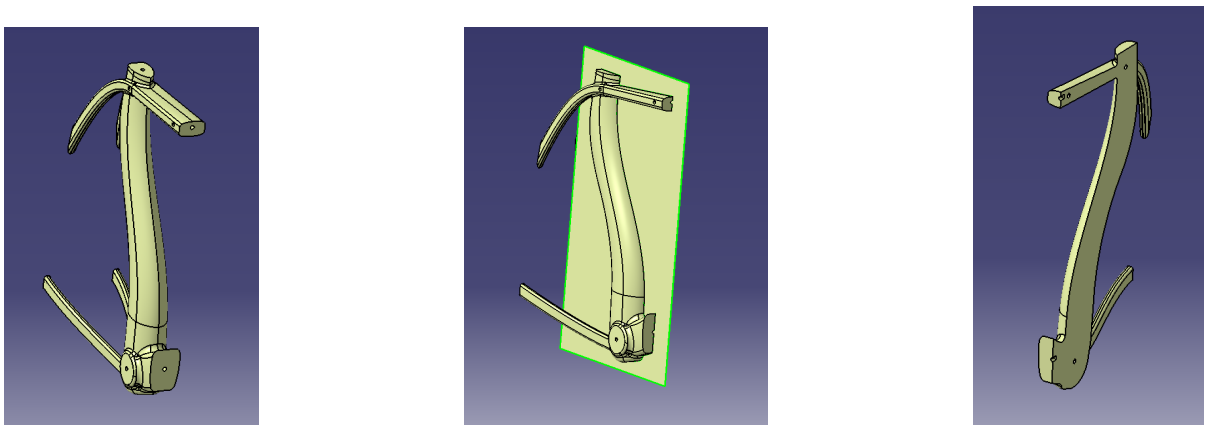

(a) Complete part **(b)** Split line **(c)** Split part

Figure 4.3: Splitting of the part

4.1.2 Scaling of the model

As the part is divided, it has to be scaled down to the required dimension. For scaling the part, it has to be converted into a solid using closed surface. After converting it into solid, the model is scaled using the scale option. These operations are carried out in part design workbench(CATIA).

4.1.3 Preparation for 3D printing

To prepare the model for 3D print it is important to convert the model into smaller triangles. Since, additive manufacturing process require triangles as the input for printing tessellation is carried out. Tessellation is a process of converting surface model into a surface of meshed triangles. These triangles can be adjusted by two parameters known as sag and step. Sag is known as the maximum distance between the triangle and step is the maximum length of the triangle. The sag value varies from 0 to 1 which determines how accurate the model is to be printed. The lower the value fine mesh is obtained, higher the value cores mesh is obtained. Once the model is tessellated it must be exported into different file format in order to read it by the printer. Generally, these models are exported into STL or STEP files. STL- Stereo Lithography or Standard Tessellation Language is a format used for 3D printing. In this format no special licence are required to import into 3D printing software. STL files can be directly imported and can be printed easily. STEP- Standard for The Exchange of Product data (ISO 10303) is also used for 3D printing. STEP files require additional support to convert the exported geometrical data into 3D printing. STL flies are used in plastic printing whereas STEP files are used in metal printing. STEP flies are used where high degree of accuracy, tolerance and dimension required over STL files.
As the model is scaled down to required dimension now, these parts need to be prepared for printing. To prepare, A copy of the solid part is extracted using extract tool. This extract is opened in a new file and is pasted as paste special in a geometrical set in order to obtain all the resulting operation of the part. Later the extracted file is tessellated for meshing purpose in STL rapid prototyping workbench. Figure 4.4 shows the tessellation of the part, where it is shown how the part is meshed into smaller triangle. This file is

exported as STL format for printing.[26]

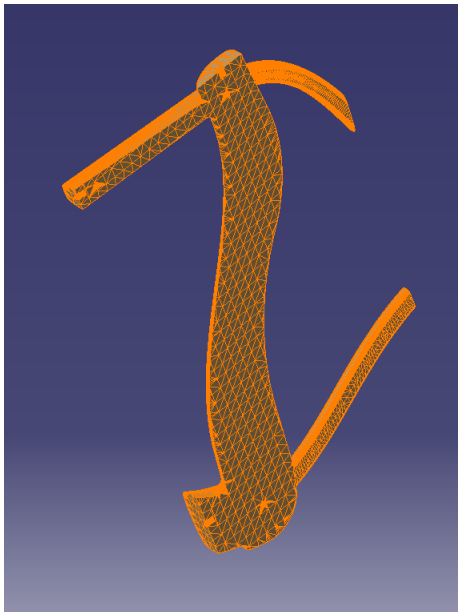

Figure 4.4: Triangle representation of the tessellated part

4.1.4 3D printing of the model

Complex designs are built easily through 3D printing. To build complex geometries, support structures are used. Support structure holds the model to the print bed. Support structures plays an important role when there is overhang, holes or complex parts in the model. The use of support structure in build is to prevent the model from falling and to transfers the heat from the model which eliminates the residual stress. The disadvantages of having support structure is post processing of the model for smoother finish, material cost and build time. To avoid support structure design optimization, optimize the part orientation or to split the model into smaller parts.
The STL file obtained from CATIA is imported into a 3D printing software called simplify 3D. In simplify 3D the exported tessellated file is placed and the orientation of the part is decided. The orientation of the part is selected in such a way that there is no support structure or minimum support structure is obtained. Along with that the amount of filling to the part, the flow rate and the speed of the printer is adjusted. The amount of fill chosen for the complete model is around 5-10%. Figure 4.5 shows the 3D printing of the bike handle with support structure.[27]

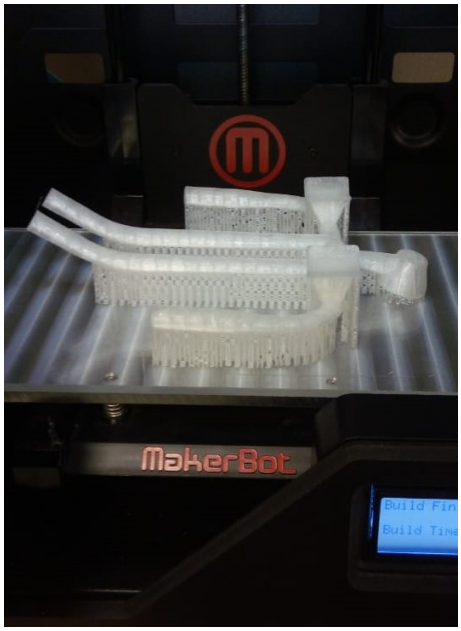

Figure 4.5: 3D printing of the bike handle with support structure

4.1.5 Assembling the model

As the model is divided into smaller parts, these smaller parts are assembled back as one complete part. Most of the parts are attached with hot glue in order to stick to each other. For the alignment of the parts that are split into half, threaded rod is used. Threaded rods are inserted through the holes for alignment and also helps to hold divided parts. Figure 4.6 shows the assembled 3D printed parts.

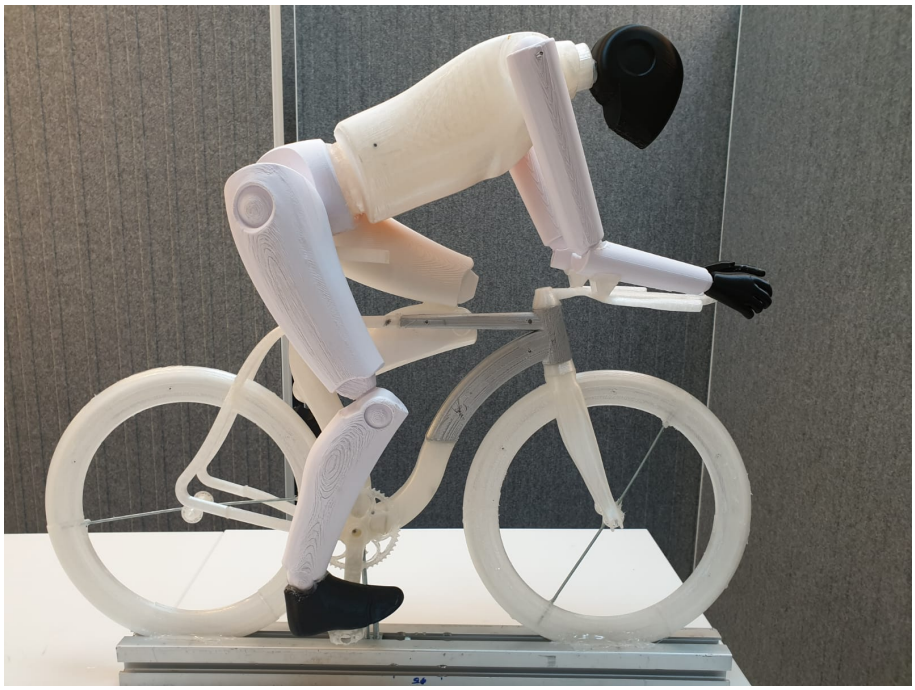

Figure 4.6: Assembled 3D printed parts

4.2 3D Printer

The printer used for 3D printing is "Makerbot Replicator 2". Makerbot replicator 2 is a single extruder printer which uses fused filament fabrication technology to print the model. Build volume of the printer is 28.5*15.3*15.5cm. It has the layer resolution up to 100-microns making the surface smooth which reduces the post-processing work. While printing the model, temperature of the extruder is set to 230°C and the print bed is set to 70°C. Figure 4.7 shows the Makerbot replicator 2 and the specification of the printer is shown in the table 4.1.[28]

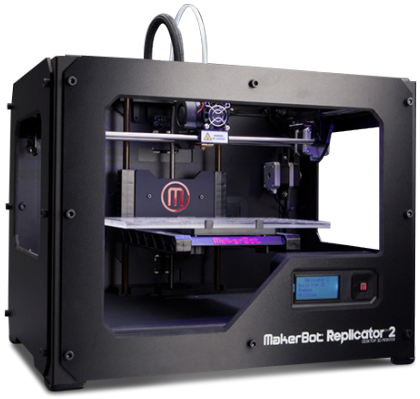

Figure 4.7: Makerbot Repliator 2 printer[29]

Printer technology	Fused Filament Fabrication
Build volume	28.5*15.3*15.5cm
Layer resolution	100,270,340microns
Filament diameter	1.75mm
Nozzle diameter	0.4mm

Table 4.1: Specification of Maker-bot Replicator 2[28]

4.3 Material selection

The most common material used for fused filament fabrication printing are, Polylactic acid commonly known as PLA. PLA is one of the most commonly used material for 3D printing. PLA is a biodegradable thermoplastic produced from the renewable resources like sugar and corn starch. PLA is environmental friendly and does not produce any toxic gases while melting. It has a glass transition temperature of 60-65°C which gives the extruded material more time to settle. PLA material does not require either the print bed or any special adhesive for 3D printing. PLA has minimal wrapping, and the reduced stress helps the material to retain its original form(structure) even after the cooling shrinkage. PLA has high strength and low printing temperature.
Acrylonitrile Butadiene Styrene Commonly known as ABS is another commonly used material for 3D printing. ABS is obtained in different grades of plastic. ABS has a glass

transition temperature of 105°C and require a print bed. Due to high transition temperature ABS causes thermal shrinkage stress during the early stages of the print and wraps out of the print bed. It has high strength and high durability.
PLA material is selected over ABS as it has the higher advantage. The material property of the PLA material is shown in the table 4.2. The values obtained are based on testing method ASTM D638.[30]

Properties	Value
Tensile strength	53 MPa
Yield strength	60 MPa
Extruder temperature	190-230°C
Bed temperature	60-70°C
printing speed	50-90mm/s

Table 4.2: Material property of PLA[31]

5

Testing

5.1 Experimental setup

The model consists of several smaller components, when combined together forms a functional prototype. Additional support is added to enhance the stability of the model in the wind tunnel at higher velocities. To reduce self induced vibrations of the model, carbon-frame support and an additional flex-link aluminum beam is used. In the wind tunnel prototype is mounted on force and moment sensors using a contact plate. Contact plate acts as a link between the prototype and the sensors below the wind-tunnel. The whole prototype is being supported by a flex link aluminum beam as shown in figure 5.1. Various 3D printed PLA parts are glued together to form a compact structure, and in some critical areas where there is instability steel rods of 3mm diameter are used.

Figure 5.1: Prototype mounted inside the wind tunnel with corresponding views

- **Flexlink:**

  To accommodate for mounting(upright) the model in the wind-tunnel, an aluminum flexlink beam is used. Flexlink beam offers flexibility to accommodate changes in the mounting setup. In this case flexlink beam is drilled with two holes, where the drilled holes are used for bolting and attaching the flexlink beam to the contact plate and the wind tunnel. Flexlink aluminum beams have grooves on each side, which allows the fasteners to slide along the grooves.

- **Carbon fibre frame**

  At higher velocities in the wind tunnel prototype tend to vibrate vigorously. To avoid undesired vibrations a carbon fibre frame is used to support to prototype. In the absence of carbon fibre frame, at higher velocities the wind tunnel measurement sensors might produce inappropriate data due to frequency interference.

- **Upright mounting**

  To keep the model upright during the whole testing duration, a threaded rod of 8mm diameter is inserted at centre of the model. The support rod serves as a major load carrier, during the testing phase in the wind tunnel. Whereas, the front tire takes only the partial load of the prototype.

5.1.1 Different configurations

Once the model is fully mounted in the wind tunnel, it is ready for testing purpose. Testing is conducted in order to determine the performance of the bike with respect to the placement of the bottle holder. To determine the performance of the bike with respect to the placement of the bottle holder four different configurations are selected. In each configuration two different types of bottle holder are placed in two different positions. The two different bottle holders are named as white bottle holder and black bottle holder. The two different positions chosen are one at the rear end of the seat post and other at the down tube of the bike. The four different configurations are,

1. **Configuration 1**
   In configuration 1 the black bottle holder is selected and is placed at the rear end of the seat post of the bike. The bottle holder is attached to the bike using zip tie. Figure 5.2a shows the configuration 1.

2. **Configuration 2**
   In configuration 2 the black bottle holder is selected and is placed at the down tube of the bike. The bottle holder is attached to the bike using zip tie. Figure 5.2b shows the configuration 2.

3. **Configuration 3**
   In configuration 3 the white bottle holder is selected and is placed at the rear end of the seat post of the bike. The bottle holder is attached to the bike using zip tie. Figure 5.2c shows the configuration 3.

4. **Configuration 4**
   In configuration 4 the white bottle holder is selected and is placed at the down tube of the bike. The bottle holder is attached to the bike using zip tie. Figure 5.2d shows the configuration 4.

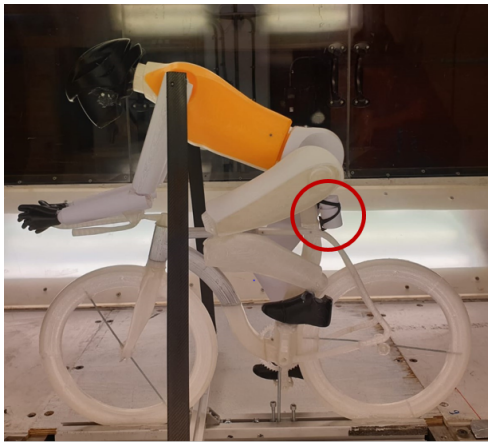

(a) Configuration 1

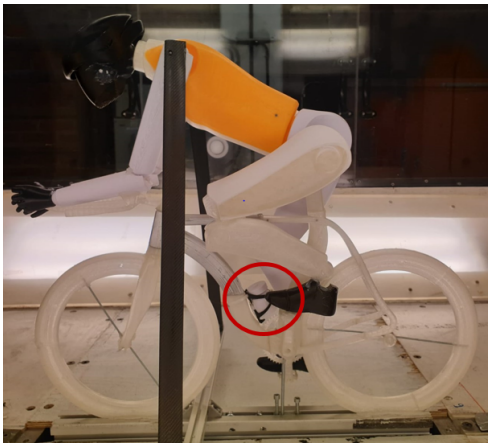

(b) Configuration 2

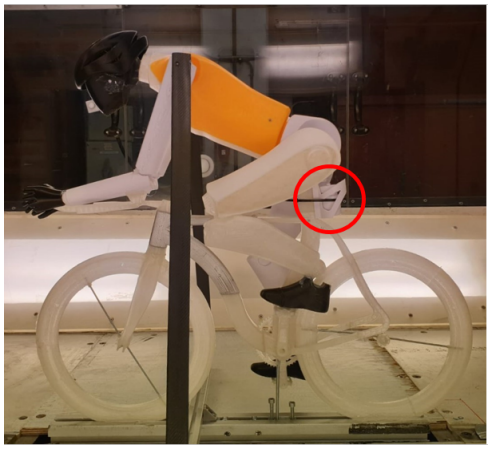

(c) configuration 3

(d) Configuration 4

Figure 5.2: Illustration of different configurations

5.2 Wind tunnel testing

5.2.1 Mounting procedure

The type of wind tunnel used for testing is a semi-closed wind tunnel, where there is no interaction with the atmospheric air. External balance and support is used for mounting the prototype for testing. Prototype is fitted firmly to the flexlink aluminum beam using slidable nuts along grooves on the top side. By using a contact plate flexlink beam along with the prototype is mounted on the balance. Contact plate consists of threaded holes in both direction which allows for fixing the threaded bolt. Once the contact plate is firmly mounted along with the prototype onto the balance, wind tunnel openings has to be completely closed to avoid any sort of disturbances caused while the body is immersed in the fluid flow.

5.2.2 Experiment procedure

To conduct the experiment prototype is mounted in the wind tunnel and all the openings are closed. Before starting the experiment, all the measurement sensors in the wind

tunnel are nullified to avoid errors. After reaching a steady state, the values are analyzed and further experimentation is continued.
Initially the velocity is set to zero and the corresponding values gained from LabVIEW are stored as text files. Then velocity is increased to 5m/s and values are stored once a steady plot is seen in LabVIEW. Experiment is further continued by gradually increasing the velocities by intervals of 5m/s up to 25m/s, and corresponding values are stored respectively. After completing all required trials the velocity is set back to zero in order to check the accuracy of the mounted setup. The experiment is conducted in three trials each in order to have a better and accurate data for analysing. Different sampling frequencies are chosen for each configuration to measure the force values. Sampling frequency chosen are 1000 Hz and 3000 Hz. The same experimental procedure is conducted for all the different configurations and the corresponding values are stored as text files. The performance of different configurations is analyzed from the obtained values by considering the mean values of the three trial data.

6

Results and analysis

6.1 Relationship between coefficient of drag and velocity

The equation for coefficient of drag and velocity is given by,

$$C_d = \frac{2D_f}{\rho \times u^2 \times A} \tag{6.1}$$

Where,
D_f = drag force acting on the body
C_d = coefficient of drag
ρ = density of the fluid inside the tunnel
A = frontal area of the body in the flow.

Since, density (ρ) and area (A) are constants w.r.t fluid and body.
From equation 6.1, coefficient of drag is directly proportional to the drag force and inversely proportional to the square of the fluid velocity. [32]

$$\text{Hence, } C_d \propto D_f \tag{6.2}$$

$$\text{Hence, } C_d \propto \frac{1}{u^2} \tag{6.3}$$

6.1.1 Comparison between Coefficient of drag and velocity

Coefficient of drag is used to determine the performance of the bike. The performance of the bike is said to be better when the coefficient of drag is low and the performance decreases as the coefficient of drag increases. From the equation 6.3, it is evident that coefficient of drag is inversely proportional to the square of the velocity and from the below graph it can be seen that the coefficient of drag decreases with respect to increase in velocity.
The performance of four configurations at sampling frequency of 1000 Hz is compared and plotted which is shown in graph 6.1. The performance of different configurations varied with respect to the change in velocity. At lower velocity the performance of configuration 2 was better than other configurations and also at higher velocity the performance of configuration 2 was better.

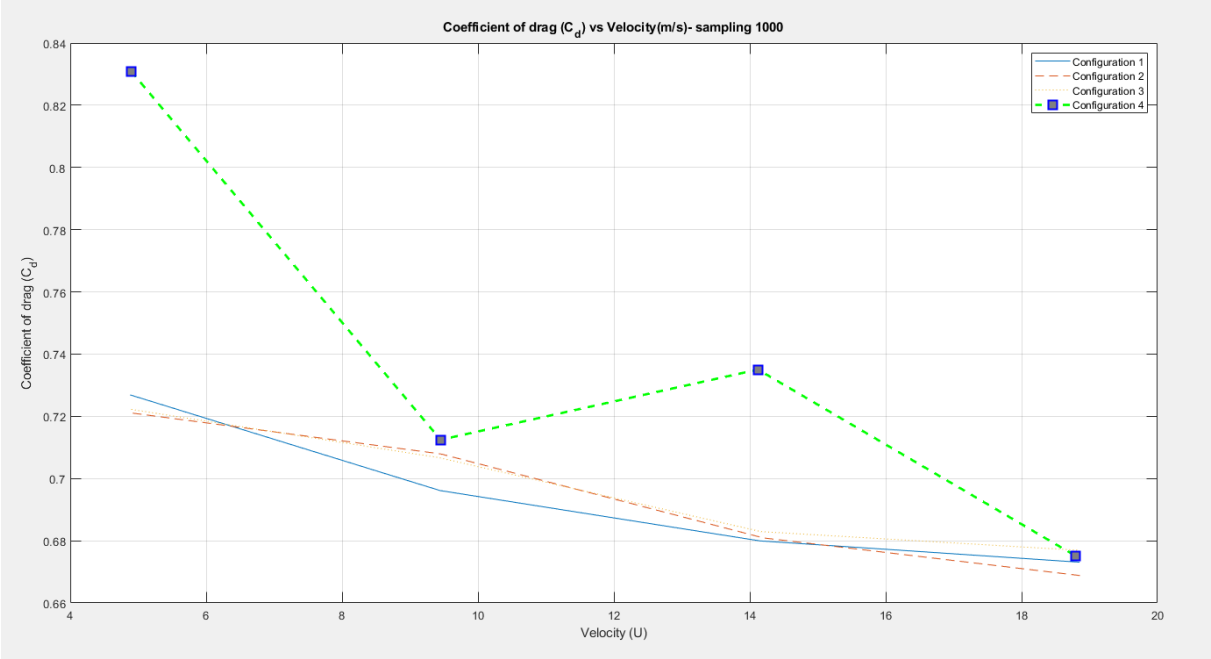

Figure 6.1: Plot of coefficient of drag and velocity, with sampling frequency 1000 Hz

But in ideal case the velocity range for bike rider tend to be around 10m/s to 14m/s. So a plot of corresponding coefficient of drag with respect to the ideal velocity range is shown in graph 6.2. In the ideal case the performance of configuration 1 was better than other configurations

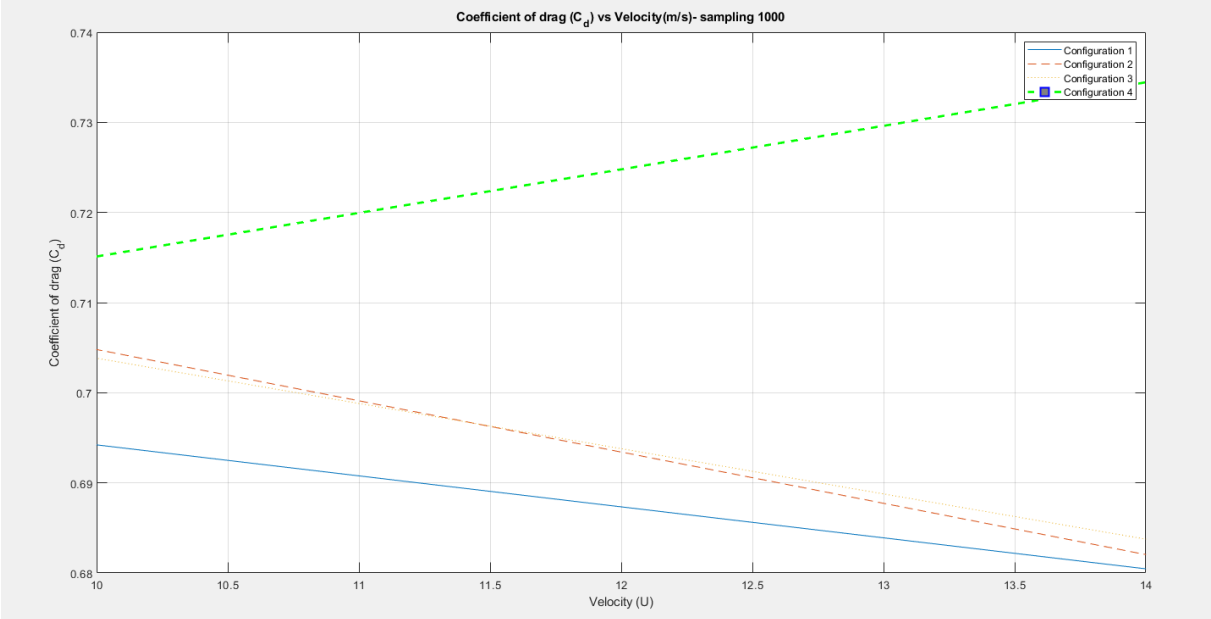

Figure 6.2: Plot of coefficient of drag and velocity, for velocity range 10m/s to 14m/s

The performance of the four configurations at sampling frequency of 3000 Hz is compared and plotted which is shown in graph 6.3. The performance of different configurations varied with respect to the change in velocity. At lower velocity the performance of configuration 4 was better. At higher velocities the performance of configuration 3 is better.

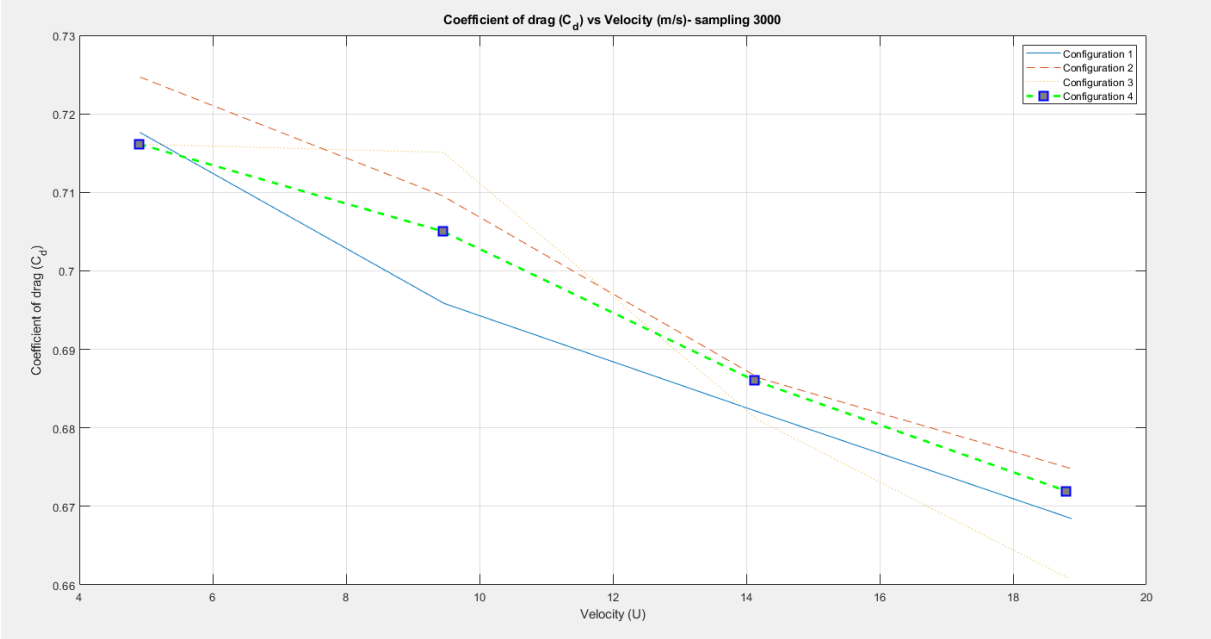

Figure 6.3: Plot of coefficient of drag and velocity, with sampling frequency 3000 Hz

The plot of coefficient of drag with respect to the ideal velocity range is shown in graph 6.4. In ideal case the performance of configuration 1 is better than other configurations

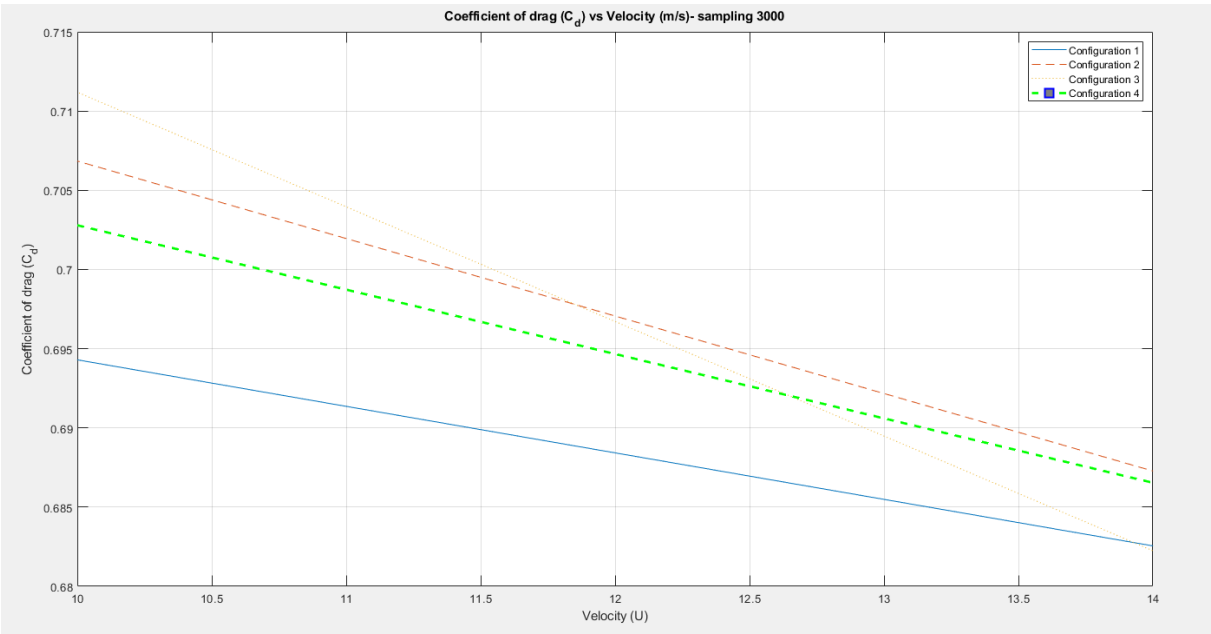

Figure 6.4: Plot of coefficient of drag and velocity, for velocity range 10m/s to 14m/s

When comparing the sampling frequency of 1000 Hz and 3000 Hz, it can be seen the coefficient of drag of different configurations at low velocity and high velocity performed differently. Where as comparing the coefficient of drag with different configurations, at ideal velocity it is seen configuration 1 performed well in both the cases.

6.2 Relationship between power, force and velocity

Power is the product of two quantities and is directly proportional to force and velocity.

$$P = F.u \tag{6.4}$$

6.2.1 Comparison of power and velocity

Power is used to determine the work done by the rider in cycling. If the power is high then the work required by the rider is high and when the power is low the work required by the rider is low. From equation 6.9 it is evident that power is directly proportional to the velocity and from the below graph it can be seen that as the velocity is increased the power increases.
The power required for four configurations at sampling frequency of 1000 Hz is compared and plotted which is shown in graph 6.5. The power required at lower and higher velocity for different configurations are same and overlapping to each other.

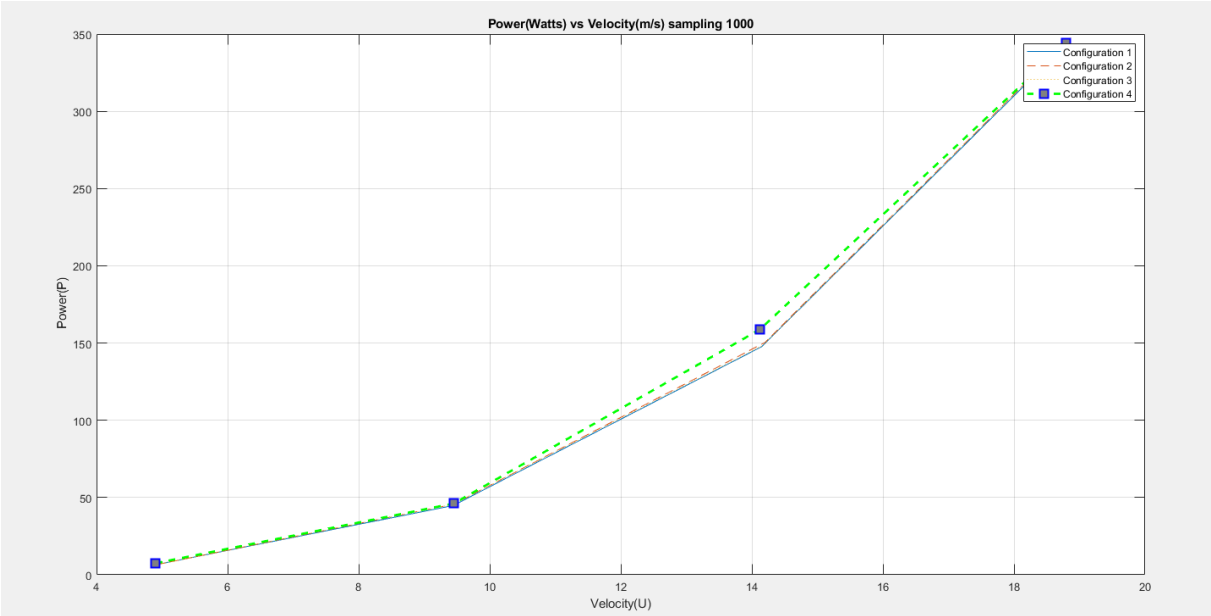

Figure 6.5: Plot of power and velocity, with sampling frequency 1000 Hz.

The plot of power with respect to the ideal velocity range is shown in graph 6.6. In ideal velocity range the power required in configuration 1 is less than other configurations.

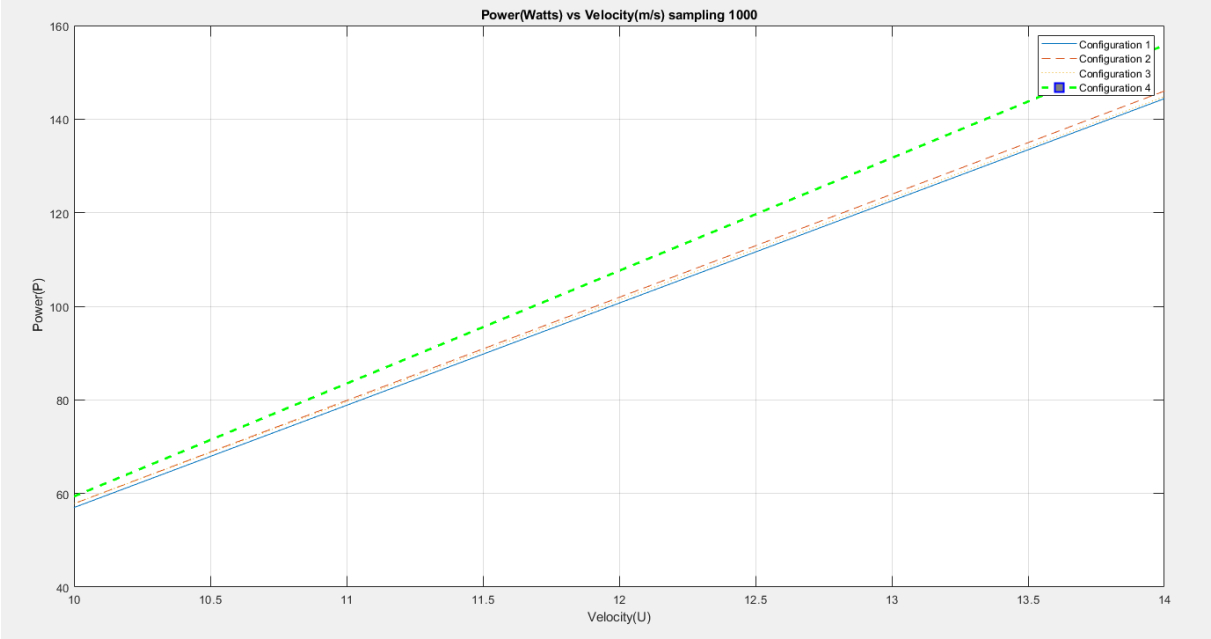

Figure 6.6: Plot of power and velocity, for velocity range 10m/s to 14m/s.

The power required for four configurations at sampling frequency of 3000 Hz is compared and plotted which is shown in graph 6.7. The power required at lower and higher velocity for different configurations are same and overlapping to each other.

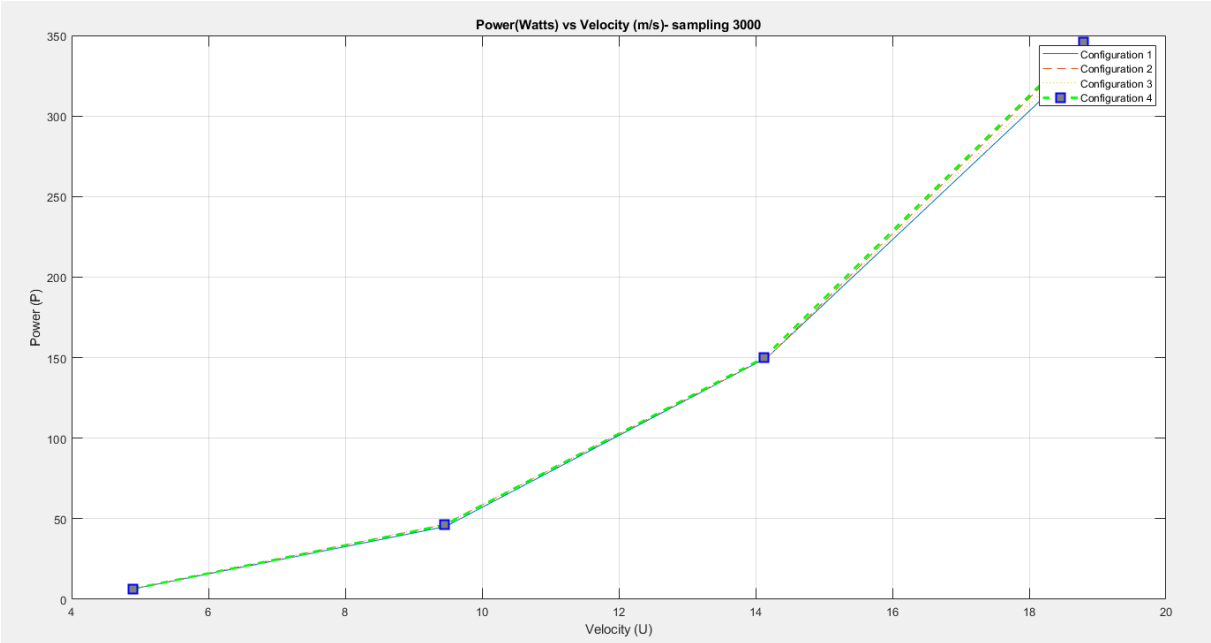

Figure 6.7: Plot of power and velocity, with sampling frequency 3000 Hz.

The plot of power with respect to the ideal velocity range is shown in graph 6.8. In ideal velocity range the power required in configuration 1 is less than other configurations.

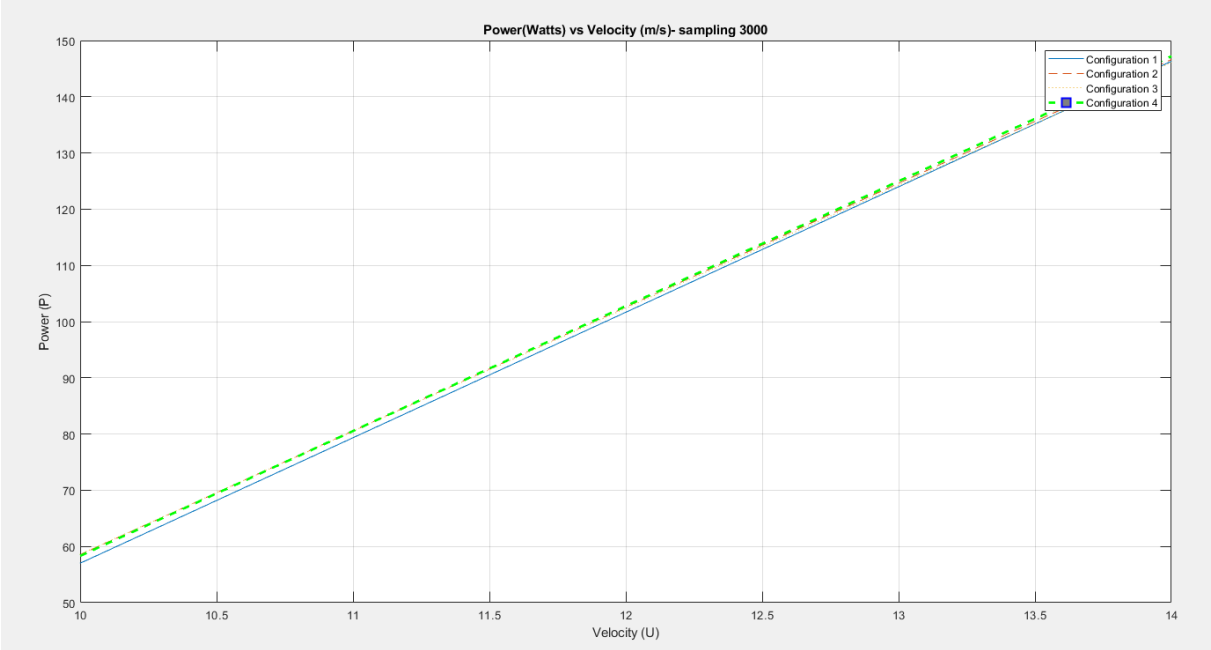

Figure 6.8: Plot of power and velocity, for velocity range 10m/s to 14m/s

When comparing both the cases of 1000 Hz and 3000 Hz, it can be seen power required for different configurations at lower velocities and higher velocities are similar. Whereas, comparing the power required for different configurations at ideal velocity range, it is seen power required by configuration 1 is less in both the cases.

7
Conclusion and Recommendation

This thesis aims to identify the impact of change in position of mounted accessories against the wind in the long run during triathlon bike phase. To analyze the impact of mounted accessories and to improve the performance of the triathlon bike a prototype is built and tested. For building prototype, replica of a triathlon bike is necessary to carry out tests in the wind tunnel. This is achieved by developing a methodology for reverse engineering. The method used for reverse engineering is to scan the physical product using a 3D scanner and obtaining the data in terms of point cloud. The obtained point cloud from scanning is converted to digital model by computing the normal and creating surface using CAD software.

After analyzing different possible solutions to convert point cloud into surface model, it was discovered that a perfect reconstructed model is difficult to obtain since most operations on point cloud is dependent on using multiple software programs and multiple file formats. When considering the results obtained, there is no major significant difference in performance of different configurations. However, for instance the amount of power required to over come a velocity of 10m/s in all the four configuration is approximately the same. Results presented may vary in real life condition since, the model is tested inside in the wind tunnel with complete isolation form atmospheric disturbances. The tested results are successful depending on the mentioned test conditions. Also, the performance parameters of the bike depends on the riders experience to generate power and balance the forces while riding long distances.[33] [34]

To conclude, accuracy of the prototype should be increased to resemble the real life scenarios as much as possible. For future development, much more different positions of the bottle and bottle holder should be tested. Besides this, additional mounted accessories and user worn equipment must be considered and tested w.r.t other factors rather than just wind as a major force component.

Bibliography

[1] International Triathlon Union Competition Rules (2016)

[2] LAURSEN P B, (2011) Long distance triathlon: demands, preparation and performance, Universidad de Alicante. Área de Educación Física y Deporte, doi:10.4100/jhse.2011.62.05

[3] Phil.Trans.R.Soc.Lond.2000 Transition to turbulent flow in aerodynamics.

[4] Raja V.(2008) Introduction to Reverse Engineering. In: Raja V., Fernandes K. (eds) Reverse Engineering. Springer Series in Advanced Manufacturing. Springer, London, DOI: 10.1007/978-1-84628-856-2

[5] Page, D. and Koschan, A and Voisin, Sophie and Ali, Ngozi and Abidi, Mongi. 3D CAD model generation of mechanical parts using coded-pattern projection and laser triangulation systems,Assembly Automation. 1999. DOI = 10.1108/01445150510610953

[6] European Community's Seventh Framework Programme, 2010. Real 3D – Digital holography for 3D and 4D real-world objects' capture, processing, and display, Deliverable 5.1 Report on the physical nature of holographic data, and on an analysis of its compatibilities with the data associated with the principal non-digital holographic 3D image acquisition and display techniques – synthesis of work from tasks 5.2-5.4, 5.7.

[7] Mostafa Abdel-Bary Ebrahim, 3D Laser Scanners' Techniques Overview,International Journal of Science and Research (IJSR), ISSN (Online): 2319-7064 Index Copernicus Value (2013): 6.14 | Impact Factor (2014): 5.611.

[8] Rusinkiewicz, S. and Levoy, M. 2000. QSplat: a multiresolution point rendering system for large meshes. In Siggraph 2000. ACM , New York, NY, 343–352. DOI= http://doi.acm.org/10.1145/344779.344940

[9] Boehler, W., Heinz, G., Marbs, A., 2001: The potential of non-contact close range laser scanners for cultural heritage recording, XVIII. CIPA Symposium, Potsdam, Germany, Proceedings.

[10] F. Remondino, "From point cloud to surface: the modeling and visualization problem," in Proceedings of the International Archives of the Photogrammetry, Remote Sensing and Spatial Information Sciences, vol. XXXIV-5/W10, 2003.

[11] Carl Erikson, Polygonal Simplification: An Overview.

[12] DeHaemer, Jr., Michael J. and Michael J. Zyda. 1991. Simplification of Objects Rendered by Polygonal Approximations. Computer Graphics, 15(2):175-184.

[13] Kuang-HuaChang,2015. Computer-Aided Engineering Design, Pages 125-167. DOI = https://doi.org/10.1016/B978-0-12-382038-9.00003-X

[14] Shiwpursad Jasveer, Xue Jianbin (2018); Comparison of Different Types of 3D Printing Technologies; International Journal of Scien-

tific and Research Publications (IJSRP) 8(4) (ISSN: 2250-3153), DOI: http://dx.doi.org/10.29322/IJSRP.8.4.2018.p7602
[15] Manufacturing 3D retrieved from:- https://manufactur3dmag.com/working-fdm-fff-3d-printing-technology/
[16] CADIMENSION retrieved from:- https://www.cadimensions.com/blog/sla-vs-polyjet-need-know/
[17] 3D printing and design retrieved from:- https://www.additive.blog/knowledge-base/3d-printers/laser-sintering-melting-sls-slm-dmls-dmp-ebm-shs/
[18] A Rajput, R.K.,2008.Fluid Mechanics Hydraulic Machines,Chand Limited.
[19] Guido Buresti, 2000. BLUFF-BODY AERODYNAMICS, WIND-EXCITED AND AEROELASTIC VIBRATIONS OF STRUCTURES.
[20] Jewel B. Barlow, William H. Rae, Jr., Alan Pope. 1999. LOW-SPEED WIND TUNNEL TESTING, THIRD EDITION.
[21] Cameron Tropea, Alexander L. Yarin, John F. Foss (Eds.), 2007. Springer Handbook of experimental fluid dynamics.
[22] Retrieved from Hexagon metrology manufacturing intelligence website
[23] Ou Yang D, Feng H, (2004) On the normal vector estimation for point cloud data from the smooth surface.
[24] Pomaska G, (2009) Utilization of Photosynth Point Clouds for 3D Object Reconstruction.
[25] Bannon, R., Parihar, S., Skarparis, Y. et al. Surg Radiol Anat (2018) 40: 185. https://doi.org/10.1007/s00276-017-1916-x
[26] Hällgren S, Pejryd L, Ekengren J.(2016) 3D data export for Additive Manufacturing - improving geometric accuracy, doi: 10.1016/j.procir.2016.05.046
[27] 3D printing support structure: a complete guide, Autonomous manufacturing, retrieved from: https://amfg.ai/2018/10/17/3d-printing-support-structures-guide
[28] Makerbot Replicator 2 brochure
[29] MatterThing retrieved from:- https://www.matterthings.com/products/makerbot-replicator-2-3d-printer-for-sale?variant=4101166017
[30] Bates-Green K, and Howie T. (2017) Materials for 3D Printing by Fused Deposition
[31] Tonerplastic, PLA 3D filament data sheet reteieved from:- https://www.dynamism.com/download/2016/tonerplastics-PLA-TDS.pdf
[32] Paul J. LaNasa, E. Loy Upp,2014. Fluid Flow Measurement (Third Edition)
[33] Jay Hoffman, 2014, Physiologial aspects of sport training and performance, Human Kinetics.
[34] Yosihiro Itai, Akira Horii, Kouichi Hirota. 1988, Relationship between the force-velocity properties developed bt consecutive muscular power and muscle fiber composition. page: 47-53, DOI = 10.2114/ahs1983.7.47.

A

Appendix

A.1 Wind tunnel data

Name	DP	U	T	Pa	rho	nu	Uhw	Tb	D
ZeroS1	0.015000	0.112650	23.84	100740	1.182	1.550498E-5	0.000000	NaN	-0.00502946750
5ms	14.080000	4.879454	23.67	100740	1.183	1.548957E-5	0.000000	NaN	-1.30061967
10ms	52.425000	9.413039	23.52	100740	1.183	1.547578E-5	0.000000	NaN	-4.72860510
15ms	117.950000	14.109141	23.10	100740	1.185	1.543684E-5	0.000000	NaN	-10.4348449
20ms	211.383333	18.878395	22.80	100740	1.186	1.540892E-5	0.000000	NaN	-18.2940377
25ms	210.850000	18.844194	22.68	100810	1.188	1.538716E-5	0.000000	NaN	-28.5770074
Zero1	0.010000	0.129862	22.87	100740	1.186	1.541530E-5	0.000000	NaN	-0.00183167157
5ms	14.045000	4.868383	23.08	100745	1.185	1.543399E-5	0.000000	NaN	-1.31531922
10ms	53.027500	9.455698	22.85	100750	1.186	1.541177E-5	0.000000	NaN	-4.76864033
15ms	119.235000	14.166330	22.32	100750	1.188	1.536313E-5	0.000000	NaN	-10.5122777
20ms	211.383333	18.856228	22.14	100750	1.189	1.534616E-5	0.000000	NaN	-18.3697157
25ms	210.850000	18.844194	22.68	100810	1.188	1.538716E-5	0.000000	NaN	-28.5770074
Zero2	0.001667	0.021623	22.37	100750	1.188	1.536805E-5	0.000000	NaN	-0.0129153424
5ms	14.250000	4.899520	22.55	100740	1.187	1.538586E-5	0.000000	NaN	-1.33560823
10ms	53.097500	9.456687	22.49	100740	1.187	1.538033E-5	0.000000	NaN	-4.78246168
15ms	119.583333	14.177754	21.91	100740	1.190	1.532651E-5	0.000000	NaN	-10.5334501
20ms	119.455000	14.166947	21.77	100740	1.190	1.531423E-5	0.000000	NaN	-10.5537498
20ms	211.175000	18.828989	21.55	100740	1.191	1.529337E-5	0.000000	NaN	-18.4149252
25ms	210.850000	18.844194	22.68	100810	1.188	1.538716E-5	0.000000	NaN	-28.5770074
ZeroS3	0.032813	0.229525	20.92	100762	1.194	1.523263E-5	0.000000	NaN	-0.00110535286
5ms	14.318125	4.911815	22.62	100740	1.187	1.539252E-5	0.000000	NaN	-1.33393959
10ms	53.153125	9.453278	21.97	100740	1.190	1.533227E-5	0.000000	NaN	-4.80223528
15ms	119.471875	14.163271	21.61	100750	1.191	1.529750E-5	0.000000	NaN	-10.5707364
20ms	212.487500	18.878153	21.27	100743	1.192	1.526711E-5	0.000000	NaN	-18.3763419
25ms	210.850000	18.844194	22.68	100810	1.188	1.538716E-5	0.000000	NaN	-28.5782862
Zero1	0.032813	0.229525	20.92	100762	1.194	1.523263E-5	0.000000	NaN	-0.00110535286
5ms	14.435938	4.926262	21.97	100750	1.190	1.533060E-5	0.000000	NaN	-1.34131998
10ms	53.283125	9.457884	21.56	100750	1.191	1.529362E-5	0.000000	NaN	-4.82926358
15ms	119.771563	14.170194	21.16	100750	1.193	1.525615E-5	0.000000	NaN	-10.5926385
20ms	212.781250	18.874031	20.75	100750	1.195	1.521874E-5	0.000000	NaN	-18.4829896
25ms	210.850000	18.844194	22.68	100810	1.188	1.538716E-5	0.000000	NaN	-28.5782862
Zero2	0.032813	0.229525	20.92	100762	1.194	1.523263E-5	0.000000	NaN	-0.00110535286
5ms	14.427187	4.921522	21.59	100755	1.191	1.529536E-5	0.000000	NaN	-1.33452347
10ms	53.717500	9.491146	21.25	100753	1.193	1.526427E-5	0.000000	NaN	-4.84172391
15ms	120.206250	14.189249	20.91	100760	1.194	1.523206E-5	0.000000	NaN	-10.6190669
20ms	213.578125	18.907304	20.72	100760	1.195	1.521410E-5	0.000000	NaN	-18.4346690
25ms	210.850000	18.844194	22.68	100810	1.188	1.538716E-5	0.000000	NaN	-28.5782862

Figure A.1: Parameters obtained form the wind tunnel

Name	DP	U	T	Pa	rho	nu	Uhw	Tb	D
ZeroS3	0.010313	0.113007	21.23	100770	1.193	1.525946E-5	0.000000	NaN	-0.0176235926
5ms	14.286250	4.900586	22.02	100770	1.190	1.533234E-5	0.000000	NaN	-1.33346661
10ms	53.114063	9.441026	21.51	100770	1.192	1.528538E-5	0.000000	NaN	-4.84650864
15ms	119.926250	14.177713	21.15	100770	1.193	1.525234E-5	0.000000	NaN	-10.7059517
20ms	213.075000	18.890084	20.90	100770	1.194	1.522975E-5	0.000000	NaN	-18.4027070
25ms	210.850000	18.844194	22.68	100810	1.188	1.538716E-5	0.000000	NaN	-28.5928616
Zero1	0.015938	0.128710	21.77	100770	1.191	1.530927E-5	0.000000	NaN	-0.00842666636
5ms	14.450625	4.927153	21.83	100770	1.190	1.531508E-5	0.000000	NaN	-1.35701073
10ms	53.240312	9.449859	21.37	100774	1.192	1.527214E-5	0.000000	NaN	-4.87204213
15ms	120.546875	14.212390	21.10	100780	1.194	1.524598E-5	0.000000	NaN	-10.6096768
20ms	212.771875	18.872124	20.76	100770	1.195	1.521681E-5	0.000000	NaN	-18.4212231
25ms	210.850000	18.844194	22.68	100810	1.188	1.538716E-5	0.000000	NaN	-28.5928616
Zero2	0.015937	0.141517	20.83	100780	1.195	1.522175E-5	0.000000	NaN	0.000476602682
5ms	14.404062	4.916326	21.49	100772	1.192	1.528363E-5	0.000000	NaN	-1.35003030
10ms	53.430625	9.462550	21.10	100771	1.193	1.524792E-5	0.000000	NaN	-4.86183308
15ms	120.701875	14.215630	20.85	100778	1.195	1.522335E-5	0.000000	NaN	-10.6088075
20ms	212.937500	18.876911	20.71	100780	1.195	1.521068E-5	0.000000	NaN	-18.4890742
25ms	210.850000	18.844194	22.68	100810	1.188	1.538716E-5	0.000000	NaN	-28.5928616
ZeroS1	0.022500	0.193266	20.84	100780	1.195	1.522221E-5	0.000000	NaN	-0.0107142606
5ms	14.491667	4.929504	21.31	100780	1.193	1.526531E-5	0.000000	NaN	-1.36086582
10ms	53.480000	9.467667	21.18	100780	1.193	1.525321E-5	0.000000	NaN	-4.90833401
15ms	120.726667	14.217358	20.86	100780	1.195	1.522466E-5	0.000000	NaN	-10.6570634
20ms	211.750000	18.823184	20.68	100780	1.195	1.520775E-5	0.000000	NaN	-18.4117589
25ms	210.850000	18.844194	22.68	100810	1.188	1.538716E-5	0.000000	NaN	-28.6029825
Zero1	0.015000	0.156207	20.92	100780	1.194	1.522933E-5	0.000000	NaN	-0.0136038716
5ms	14.420000	4.916579	21.22	100780	1.193	1.525735E-5	0.000000	NaN	-1.35735497
10ms	53.529167	9.470367	21.07	100780	1.194	1.524380E-5	0.000000	NaN	-4.89087769
15ms	120.795000	14.216333	20.65	100780	1.195	1.520546E-5	0.000000	NaN	-10.6317228
20ms	214.141667	18.925830	20.59	100784	1.196	1.519871E-5	0.000000	NaN	-18.4636595
25ms	210.850000	18.844194	22.68	100810	1.188	1.538716E-5	0.000000	NaN	-28.6029825
Zero	0.020000	0.181925	20.77	100781	1.195	1.521627E-5	0.000000	NaN	-0.0125288709
Zero2	0.020000	0.181925	20.77	100781	1.195	1.521627E-5	0.000000	NaN	-0.0125288709
5ms	14.517500	4.931986	21.11	100790	1.194	1.524550E-5	0.000000	NaN	-1.35197304
10ms	53.195833	9.438185	20.94	100790	1.194	1.522981E-5	0.000000	NaN	-4.88017402
15ms	120.563333	14.204042	20.74	100790	1.195	1.521175E-5	0.000000	NaN	-10.5857152
20ms	213.100000	18.880446	20.63	100790	1.196	1.520135E-5	0.000000	NaN	-18.4026181
25ms	210.850000	18.844194	22.68	100810	1.188	1.538716E-5	0.000000	NaN	-28.6029825

Figure A.2: Parameters obtained form the wind tunnel

Name	DP	U	T	Pa	rho	nu	Uhw	Tb	p
ZeroS1	0.065000	0.328669	22.74	100800	1.187	1.539375E-5	0.000000	NaN	-0.00770419730
5ms	14.548333	4.948537	22.49	100800	1.188	1.537102E-5	0.000000	NaN	-1.32926166
10ms	52.934167	9.428231	21.81	100804	1.191	1.530778E-5	0.000000	NaN	-4.81539026
15ms	119.215000	14.141833	21.50	100800	1.192	1.527959E-5	0.000000	NaN	-10.4690445
20ms	210.796667	18.800859	21.38	100803	1.193	1.526821E-5	0.000000	NaN	-18.4048071
25ms	210.850000	18.844194	22.68	100810	1.188	1.538716E-5	0.000000	NaN	-28.6279034
Zero1	0.014167	0.151868	21.47	100800	1.192	1.527730E-5	0.000000	NaN	-0.00873995876
5ms	14.176667	4.878584	21.75	100810	1.191	1.530153E-5	0.000000	NaN	-1.33494665
10ms	52.896667	9.420216	21.53	100810	1.192	1.528168E-5	0.000000	NaN	-4.84176184
15ms	118.655000	14.103081	21.29	100808	1.193	1.525939E-5	0.000000	NaN	-10.4919077
20ms	211.523333	18.827601	21.22	100810	1.193	1.525281E-5	0.000000	NaN	-18.4348239
25ms	210.850000	18.844194	22.68	100810	1.188	1.538716E-5	0.000000	NaN	-28.6279034
Zero2	0.014167	0.151868	21.47	100800	1.192	1.527730E-5	0.000000	NaN	-0.00873995876
5ms	14.413333	4.917634	21.57	100810	1.192	1.528497E-5	0.000000	NaN	-1.34570093
10ms	53.428333	9.465087	21.39	100811	1.193	1.526823E-5	0.000000	NaN	-4.83797510
15ms	119.453333	14.146405	21.13	100810	1.194	1.524423E-5	0.000000	NaN	-10.5843800
20ms	210.148333	18.762520	21.10	100810	1.194	1.524194E-5	0.000000	NaN	-18.4085489
25ms	210.850000	18.844194	22.68	100810	1.188	1.538716E-5	0.000000	NaN	-28.6279034
ZeroS3	0.009063	0.117332	21.29	100810	1.193	1.525950E-5	0.000000	NaN	-0.00238608634
5ms	14.406875	4.917272	21.66	100810	1.192	1.529316E-5	0.000000	NaN	-1.33089051
10ms	52.939375	9.420661	21.32	100810	1.193	1.526228E-5	0.000000	NaN	-4.82090477
15ms	119.975937	14.177790	21.14	100807	1.194	1.524567E-5	0.000000	NaN	-10.5814216
20ms	211.680000	18.831376	21.11	100807	1.194	1.524332E-5	0.000000	NaN	-18.4459277
25ms	210.850000	18.844194	22.68	100810	1.188	1.538716E-5	0.000000	NaN	-28.6883874
Zero1	0.010000	0.129471	21.30	100810	1.193	1.525987E-5	0.000000	NaN	-0.00659973908
5ms	14.422187	4.918947	21.54	100807	1.192	1.528250E-5	0.000000	NaN	-1.33767789
10ms	53.740625	9.490009	21.25	100810	1.193	1.525539E-5	0.000000	NaN	-5.20039648
15ms	119.692500	14.160458	21.11	100805	1.194	1.524329E-5	0.000000	NaN	-10.5918043
20ms	210.210937	18.763840	21.06	100810	1.194	1.523831E-5	0.000000	NaN	-17.5212313
25ms	210.850000	18.844194	22.68	100810	1.188	1.538716E-5	0.000000	NaN	-28.6883874
Zero2	0.006875	0.089023	21.40	100814	1.193	1.526918E-5	0.000000	NaN	-0.00554943221
5ms	14.352813	4.907018	21.57	100820	1.192	1.528343E-5	0.000000	NaN	-1.33489753
10ms	53.144375	9.439919	21.42	100820	1.193	1.526938E-5	0.000000	NaN	-4.84068058
15ms	119.581250	14.158784	21.36	100820	1.193	1.526375E-5	0.000000	NaN	-10.5570861
20ms	211.403750	18.828380	21.44	100820	1.193	1.527151E-5	0.000000	NaN	-18.4563680
25ms	210.850000	18.844194	22.68	100810	1.188	1.538716E-5	0.000000	NaN	-28.6883874

Figure A.3: Parameters obtained form the wind tunnel

Name	DP	U	T	Pa	rho	nu	Uhw	Tb	D
zeroS1	0.006875	0.089111	21.98	100813	1.190	1.532232E-5	0.000000	NaN	-0.00895591841
5ms	14.459687	4.930417	22.19	100820	1.190	1.534021E-5	0.000000	NaN	-1.35797682
10ms	53.187500	9.452060	21.94	100820	1.191	1.531711E-5	0.000000	NaN	-4.92152457
15ms	121.359375	14.273944	21.85	100820	1.191	1.530891E-5	0.000000	NaN	-11.4823180
20ms	210.554375	18.805286	21.90	100820	1.191	1.531409E-5	0.000000	NaN	-18.3598258
25ms	210.850000	18.844194	22.68	100810	1.188	1.538716E-5	0.000000	NaN	-28.7637124
zero1	0.019375	0.176844	22.02	100810	1.190	1.532605E-5	0.000000	NaN	-0.0112718790
5ms	14.982188	5.015720	22.13	100810	1.190	1.533641E-5	0.000000	NaN	-1.61914980
10ms	52.615000	9.403355	22.05	100810	1.190	1.532919E-5	0.000000	NaN	-4.85901401
15ms	122.035000	14.316040	21.96	100810	1.190	1.532113E-5	0.000000	NaN	-11.6347832
20ms	211.100000	18.835941	22.07	100810	1.190	1.533109E-5	0.000000	NaN	-18.3809042
25ms	210.850000	18.844194	22.68	100810	1.188	1.538716E-5	0.000000	NaN	-28.7637124
zero2	0.006875	0.089159	22.23	100800	1.189	1.534722E-5	0.000000	NaN	-0.00637408435
5ms	14.657500	4.964323	22.34	100800	1.189	1.535712E-5	0.000000	NaN	-1.63219050
10ms	53.349375	9.472675	22.27	100800	1.189	1.535053E-5	0.000000	NaN	-4.89585072
15ms	120.061250	14.209582	22.23	100800	1.189	1.534702E-5	0.000000	NaN	-10.6253455
20ms	210.856875	18.834030	22.33	100803	1.189	1.535627E-5	0.000000	NaN	-18.1721576
25ms	210.850000	18.844194	22.68	100810	1.188	1.538716E-5	0.000000	NaN	-28.7637124
ZeroS3	0.055000	0.303990	22.59	100810	1.188	1.537932E-5	0.000000	NaN	-0.0134255922
5ms	14.445000	4.930935	22.52	100810	1.188	1.537210E-5	0.000000	NaN	-1.35159626
10ms	52.830000	9.430103	22.50	100800	1.188	1.537163E-5	0.000000	NaN	-4.88345308
15ms	119.430000	14.177889	22.50	100810	1.188	1.537011E-5	0.000000	NaN	-10.5504154
20ms	210.536667	18.825303	22.53	100810	1.188	1.537303E-5	0.000000	NaN	-18.3564397
25ms	210.850000	18.844194	22.68	100810	1.188	1.538716E-5	0.000000	NaN	-28.7390750
Zero1	0.010000	0.129776	22.69	100810	1.188	1.538769E-5	0.000000	NaN	-0.00139430768
5ms	14.297500	4.907205	22.70	100810	1.187	1.538885E-5	0.000000	NaN	-1.34272145
10ms	53.160000	9.462935	22.74	100810	1.187	1.539253E-5	0.000000	NaN	-4.91201358
15ms	119.435000	14.182762	22.69	100810	1.188	1.538769E-5	0.000000	NaN	-10.5936465
20ms	210.720000	18.838171	22.67	100810	1.188	1.538654E-5	0.000000	NaN	-18.3364721
25ms	210.850000	18.844194	22.68	100810	1.188	1.538716E-5	0.000000	NaN	-28.7390750
zero2	210.850000	18.844194	22.68	100810	1.188	1.538716E-5	0.000000	NaN	-0.00280453204
5ms	210.850000	18.844194	22.68	100810	1.188	1.538716E-5	0.000000	NaN	-1.32704807
10ms	210.850000	18.844194	22.68	100810	1.188	1.538716E-5	0.000000	NaN	-4.87580115
15ms	210.850000	18.844194	22.68	100810	1.188	1.538716E-5	0.000000	NaN	-10.5999888
20ms	210.850000	18.844194	22.68	100810	1.188	1.538716E-5	0.000000	NaN	-18.4494089
25ms	210.850000	18.844194	22.68	100810	1.188	1.538716E-5	0.000000	NaN	-28.7390750

Figure A.4: Parameters obtained form the wind tunnel

A.2 Relationship between drag force and velocity

Factors affecting the relationship between drag force and velocity is given by the equation as follows,

$$D_f = \frac{C_d \times \rho \times A \times u^2}{2} \tag{A.1}$$

It is evident from equation,
Drag force D_f is directly proportional to square of the velocity(U) and Coefficient of drag (C_d).
Mathematically,

$$D_f = \frac{(C_d \times u^2) \times (A \times \rho)}{2} \tag{A.2}$$

Since, density (ρ) and area (A) are constant for the fluid and the model it can eliminated with a proportionality relationship.[3] & [32]

$$\because (\frac{A \times \rho}{2}) = \text{Constant for the whole testing phase.} \tag{A.3}$$

$$\text{Hence,} D_f \propto (C_d \times u^2) \tag{A.4}$$

A.2.1 Comparison between drag force and velocity

From the above equations, it is evident that drag force is proportional to square of the velocity and from the plots below the it can be seen that drag force increases exponentially w.r.t increase in velocity. Out of the four configurations, first configuration tends to perform well against the drag force whereas fourth configuration has significant increase in drag force along with increase in velocity.

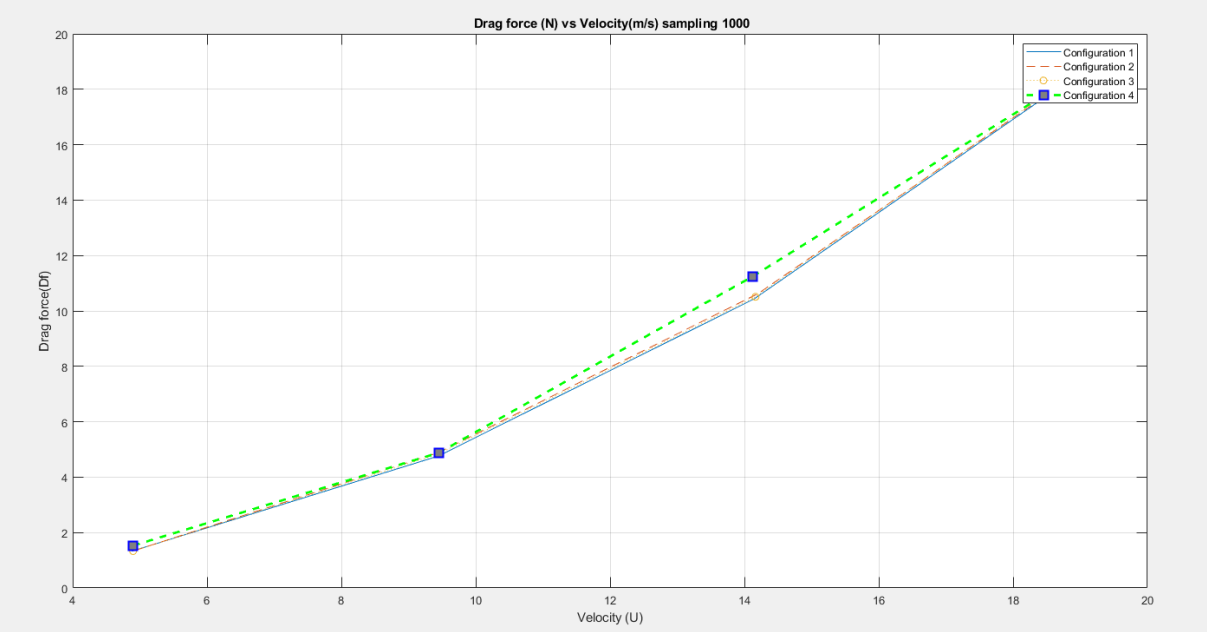

Figure A.5: Plot of drag force vs velocity, with sampling frequency 1000 Hz

Ideal velocity range for bike riders is tend to be around 10m/s to 14m/s so a plot corresponding to mentioned velocity range is shown below. When considering the amount of drag force generated from increase in velocity is significant in all the cases. From the plot it is clear that first configuration performs is better.

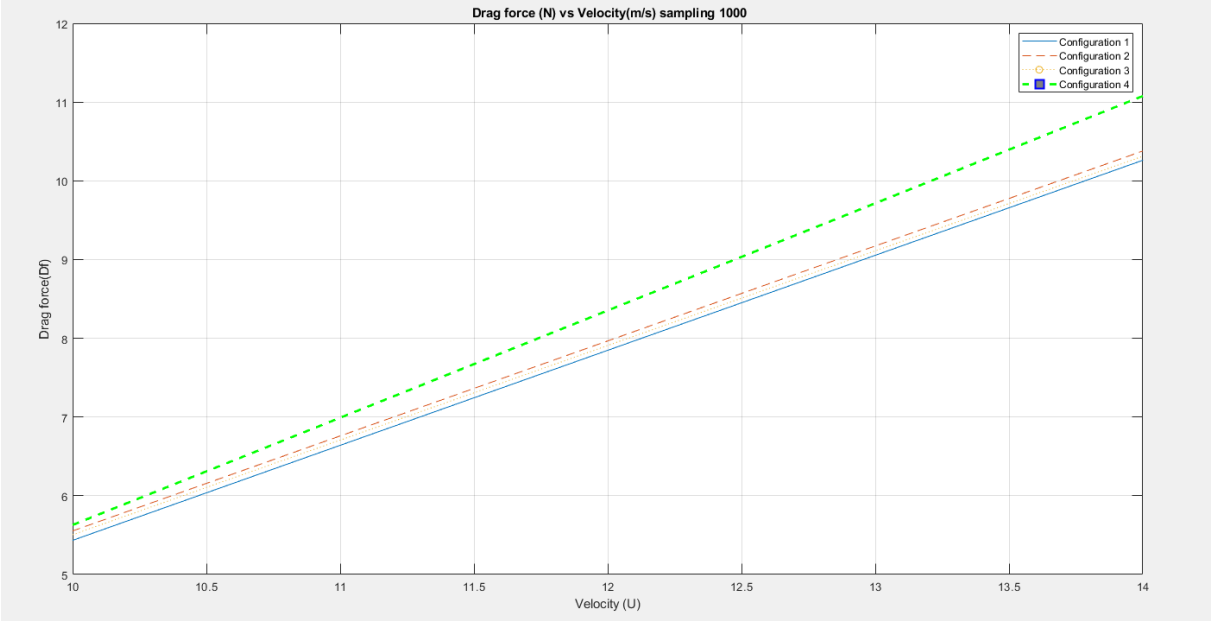

Figure A.6: Plot of drag force vs velocity, for velocity range 10m/s to 14m/s

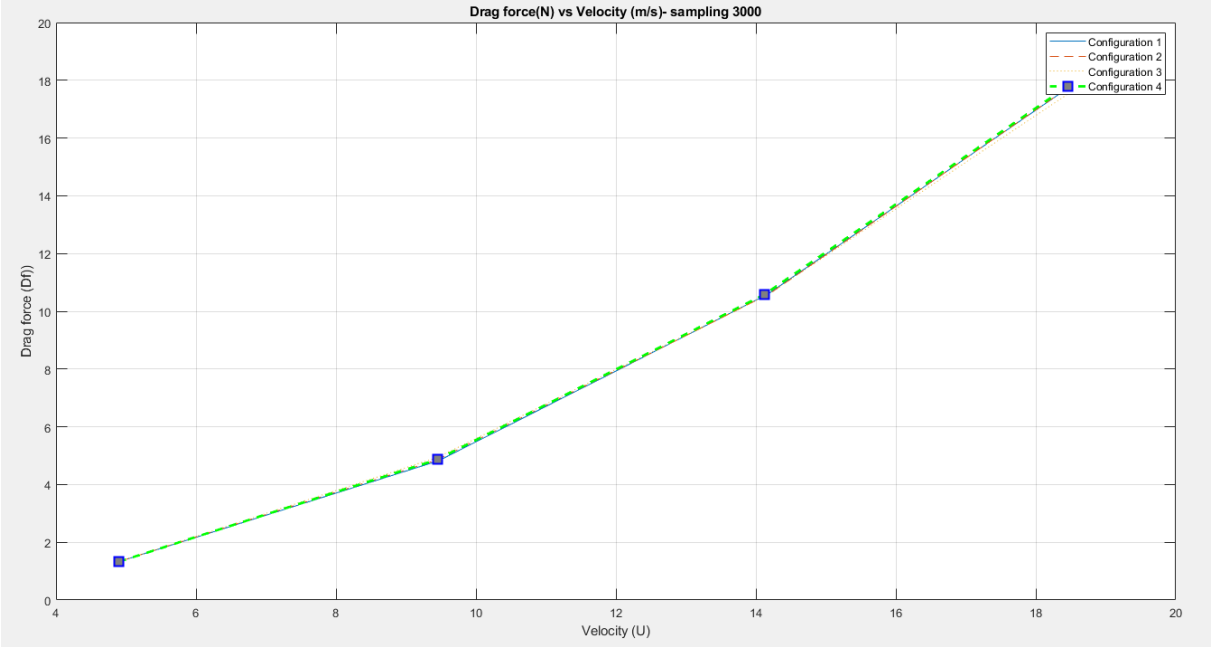

Figure A.7: Plot of drag force vs velocity, with sampling frequency 3000Hz

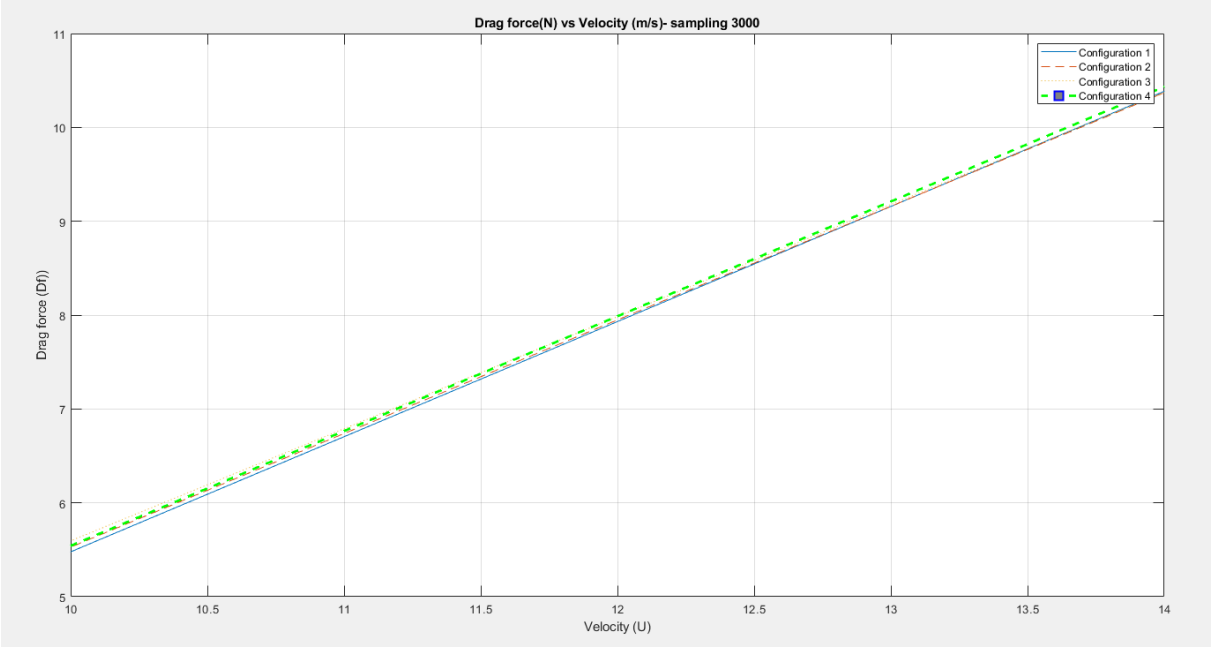

Figure A.8: Plot of drag force vs velocity, for velocity range 10m/s to 14m/s

The above plots A.7 and A.8 depict the same results as the above. The only difference being in the measuring frequency of 1000 and 3000 Hz, which means the values is being measured every $\frac{1}{1000}th$ of second in 1000 Hz and every $\frac{1}{3000}th$ of a second.

A.3 Comparison of power and drag force

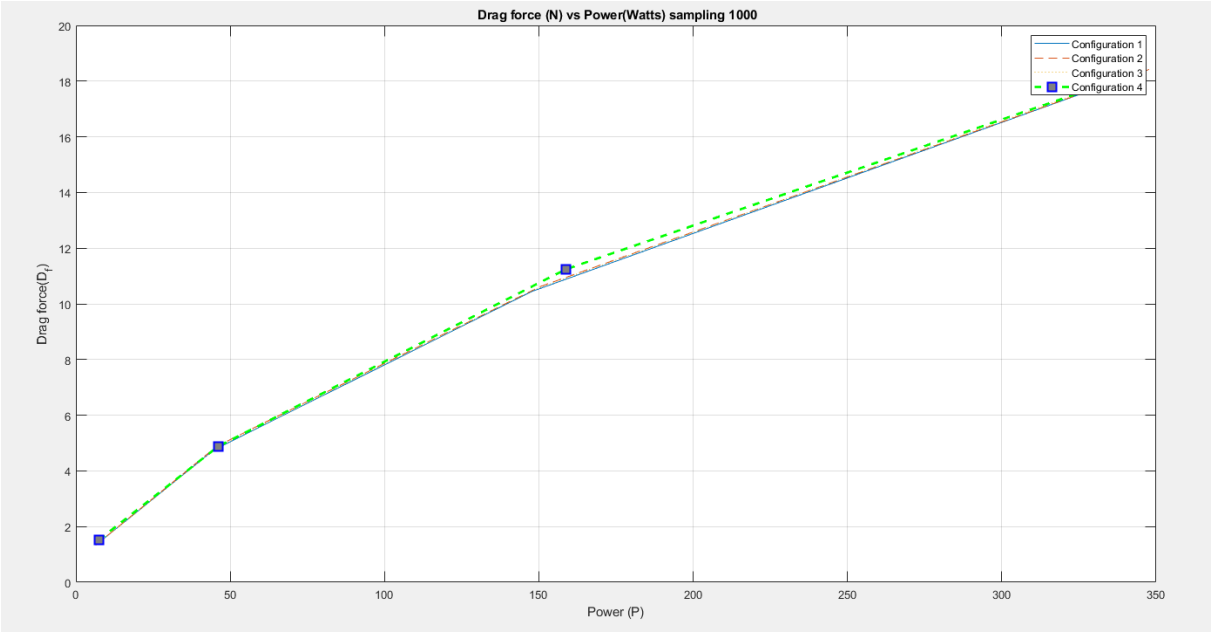

Figure A.9: Plot of power vs drag force, with sampling frequency 1000 Hz.

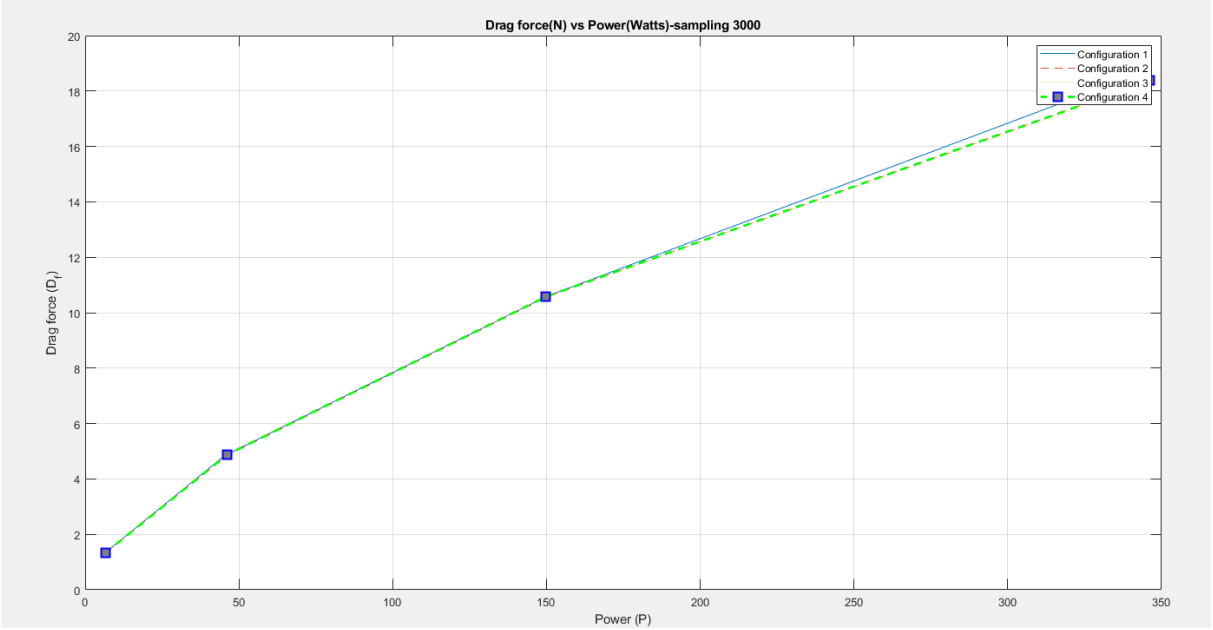

Figure A.10: Plot of power vs drag force, with sampling frequency 3000 Hz.